frontiers in Earth Science

ORIGINAL RESEARCH
published: 07 December 2021
doi: 10.3389/feart.2021.772083

Origin and Characteristics of the Shwetagun Deposit, Modi Taung-Nankwe Gold District and the Kunzeik and Zibyaung Deposits, Kyaikhto Gold District in Mergui Belt, Myanmar: Implications for Fluid Source and Orogenic Gold Mineralization

Myo Kyaw Hlaing[1,2]*, *Kotaro Yonezu*[1], *Khin Zaw*[3], *Aung Zaw Myint*[2], *May Thwe Aye*[2] and *Koichiro Watanabe*[1]

[1]Department of Earth Resources Engineering, Kyushu University, Fukuoka, Japan, [2]Department of Geology, University of Yangon, Yangon, Myanmar, [3]Centre of Ore Deposits and Earth Sciences, School of Natural Sciences, University of Tasmania, Hobart, TAS, Australia

OPEN ACCESS

Edited by:
David R Lentz,
University of New Brunswick
Fredericton, Canada

Reviewed by:
Mohd Basril Iswadi Basori,
National University of Malaysia,
Malaysia
Thierry Bineli Betsi,
Botswana International University of
Science and Technology, Botswana

***Correspondence:**
Myo Kyaw Hlaing
myokyawhlaing.edu.geol@
gmail.com

Specialty section:
This article was submitted to
Economic Geology,
a section of the journal
Frontiers in Earth Science

Received: 07 September 2021
Accepted: 16 November 2021
Published: 07 December 2021

Citation:
Hlaing MK, Yonezu K, Zaw K, Myint AZ, Aye MT and Watanabe K (2021) Origin and Characteristics of the Shwetagun Deposit, Modi Taung-Nankwe Gold District and the Kunzeik and Zibyaung Deposits, Kyaikhto Gold District in Mergui Belt, Myanmar: Implications for Fluid Source and Orogenic Gold Mineralization.
Front. Earth Sci. 9:772083.
doi: 10.3389/feart.2021.772083

The Mergui Belt of Myanmar is endowed with several important orogenic gold deposits, which have economic significance and exploration potential. The present research is focused on two gold districts, Modi Taung-Nankwe and Kyaikhto in the Mergui Belt comparing their geological setting, ore and alteration mineralogy, fluid inclusion characteristics, and ore-forming processes. Both of the gold districts show similarities in nature and characteristics of gold-bearing quartz veins occurring as sheeted veins, massive veins, stockworks to spider veinlets. These gold deposits are mainly hosted by the mudstone, slaty mudstone, greywacke sandstone, slate, and slaty phyllite of Mergui Group (dominantly of Carboniferous age). The gold-bearing quartz veins generally trend from NNE to N-S, whereas some veins strike NW-SE in all deposits. The gold-bearing quartz veins are mainly occurred within the faults and shear zones throughout the two gold districts. Wall-rock alterations at Shwetagun are mainly silicification, chloritization, and sericitization, whereas in Kyaikhto, silicification, carbonation, as well as chloritization, and sericitization are common. At Shwetagun, the gold occurred as electrum grains in fractures within the veins and sulfides. In Kyaikhto, the quartz-carbonate-sulfide and quartz-sulfide veins appeared to have formed from multiple episodes of gold formation categorizing mainly as free native gold grains in fractures within the veins or invisible native gold and electrum within sulfides. At Shwetagun, the ore minerals in the auriferous quartz veins include pyrite, galena, and sphalerite, with a lesser amount of electrum, chalcopyrite, arsenopyrite, chlorite, and sericite. In Kyaikhto, the common mineralogy associated with gold mineralization is pyrite, chalcopyrite, sphalerite, galena, pyrrhotite, arsenopyrite, marcasite, magnetite, hematite, ankerite, calcite, chlorite, epidote, albite, and sericite.

At Shwetagun, the mineralization occurred at a varying temperature from 250 to 335°C, with a salinity range from 0.2 to 4.6 wt% NaCl equivalent. The Kyaikhto gold district was formed from aqueous–carbonic ore fluids of temperatures between 242 and 376°C, low to medium salinity (<11.8 wt% NaCl equivalent), and low CO_2 content. The ore-forming processes of the Shwetagun deposit in the Modi Taung-Nankwe gold district and the Kyaikhto gold district are remarkably comparable to those of the mesozonal orogenic gold systems.

Keywords: Shwetagun, Kyaikhto, Mergui belt, Mesozonal, Orogenic gold systems

INTRODUCTION

The Mergui Belt (MB) is one of the largest and most economically important gold provinces in Myanmar. This belt has a diverse style of mineralization in Myanmar such as orogenic gold deposits (e.g., Modi Taung), vein-type tin and tungsten deposits (e.g., Hermyingyi), and stratabound antimony deposits (e.g., Kaw Hket–Taunggalay–Htimiwa) (Ye Myint Swe et al., 2017; Khin Zaw, 2017; Mitchell, 2018). The MB was intruded by several granitic rocks of the Central Granite Belt of Myanmar (Khin Zaw, 1990) which extends into peninsular Thailand, and these granites form part of the Western Granite Province of Southeast Asian Tin Belts (Cobbing et al., 1986, 1992). The northern part of MB is characterized by high-grade metamorphic rocks such as gneiss, granitoid gneiss, marble, and calc-silicates associated with Late Proterozoic to Mesozoic sedimentary sequences. The southern part of MB consists of Upper Carboniferous to Lower Permian metasedimentary rocks of predominantly Mergui Group and the rocks are metamorphosed to greenschist facies with small zones of amphibolite facies along the margins of the belt, close to major shear zones and granite intrusions (**Figures 1**, **2**; Cobbing et al., 1986, 1992; Schwartz et al., 1995; Mitchell et al., 1999, Mitchell et al., 2004, Mitchell et al., 2007, 2012; Khin Zaw, 1990; 2017, 2019; Khin Zaw et al., 2014a, 2018; Ye Myint Swe et al., 2017; Mitchell, 2018; Myo Kyaw Hlaing et al., 2019).

Orogenic gold deposits are one of the main groups of gold deposits making up a major source of gold produced worldwide (e.g., Groves et al., 1998; Dubé and Gosselin, 2007). They occur in convergent plate margins in accretionary and collisional orogens, indicating subduction-related metamorphic (thermal events) processes in deep-crustal environments (Barley and Groves, 1992; Groves et al., 1998; Goldfarb et al., 2004, 2005; Bierlein et al., 2006, 2009; Groves and Bierlein, 2007). These gold deposits are typically hosted by rocks of greenschist to amphibolite metamorphic grade, and locally up to granulite facies conditions of various ages, displaying variable degrees of deformation (Groves, 1993; Groves et al., 1998, 2003; Goldfarb et al., 2001, 2005, 2015; Connolly, 2010; Tomkins, 2010). Giant orogenic gold deposits are commonly located in second-order structures linked to shear zones and lithospheric-scale faults, indicating first-order fluid conduits (McCuaig et al., 2010; Groves et al., 2018; Davies et al., 2019).

The occurrences of the orogenic gold deposits in Myanmar have been recorded in the form of gold-quartz veins at the Tatlet, Phayaung Taung, Nankwe, Modi Taung, Shwegyin, Kyaiktho, and Russell Island (Shwekyun) areas within the MB (Ye Myint Swe et al., 2017). The belt has been exploited with a combination of the historical and currently available resources and reserves totaling around 4.92 Mt Au (**Figure 1**; Mitchell et al., 1999, 2004; Ye Myint Swe et al., 2017 and references therein). The Shwetagun deposit in the Modi Taung-Nankwe gold district and the Kunzeik, Zibaung and Meyon deposits in the Kyaikhto gold district are located in central to southern parts of Myanmar along the MB (**Figures 1**, **2**; Mitchell et al., 1999, 2004; Ye Myint Swe et al., 2017).

Previous studies on the gold deposits of the MB have only focused on the general geology of central to southern parts of Myanmar, and there is a lack of systematic studies on the district-scale to local geology, geochemistry, ore mineralogy and genesis, and ore-controlling structures of gold deposits in the interior of the Mergui Belt, which limits our knowledge of gold mineralization and the metallogenic process. Here we compare the nature and setting of gold mineralization of the Shwetagun deposit from the Modi Taung-Nankwe gold district with the Kunzeik, Zibaung and Meyon gold deposits from the Kyaikhto gold district and discuss the conditions of ore formation and metallogenesis in a regional tectonic framework based on geology, ore characteristics, alteration mineralogy, and fluid inclusion studies.

REGIONAL GEOLOGIC SETTING

The gold deposits of Myanmar comprise six major north-south trending geological linkages or tectonic terranes/belts (**Figure 1**). The Mogok-Mandalay-Mergui Belt (MMMB) is exposed in a 1,300 km long belt of 20–100 km in width at the western margin of the Sibumasu (**Figures 1**, **2**; Bender, 1983; Mitchell et al., 2004; Gardiner et al., 2014, 2018; Mitchell, 2018). The southern part of MMMB is defined here as Mergui Belt (MB) and it is also known as Slate Belt in Myanmar. We used the term MB as the Slate Belt is a misnomer due to the presence of abundant other lithologies such as sandstones, carbonaceous siltstones, greywackes, and calcareous mudstones rather than slate unit. These lithologies belong to the Mergui Group, running a distinctly north-south direction from Mandalay towards Dawei (Tavoy) and Myeik (Mergui) and southeastward through Phuket, southern Thailand, and eastern Sumatra to Bangka Island in Indonesia. This belt is made up of interbedded slaty mudstones, slate and pebbly wackes, less abundant quartzites, and rare calcareous beds, and the northern part of the belt extend an additional

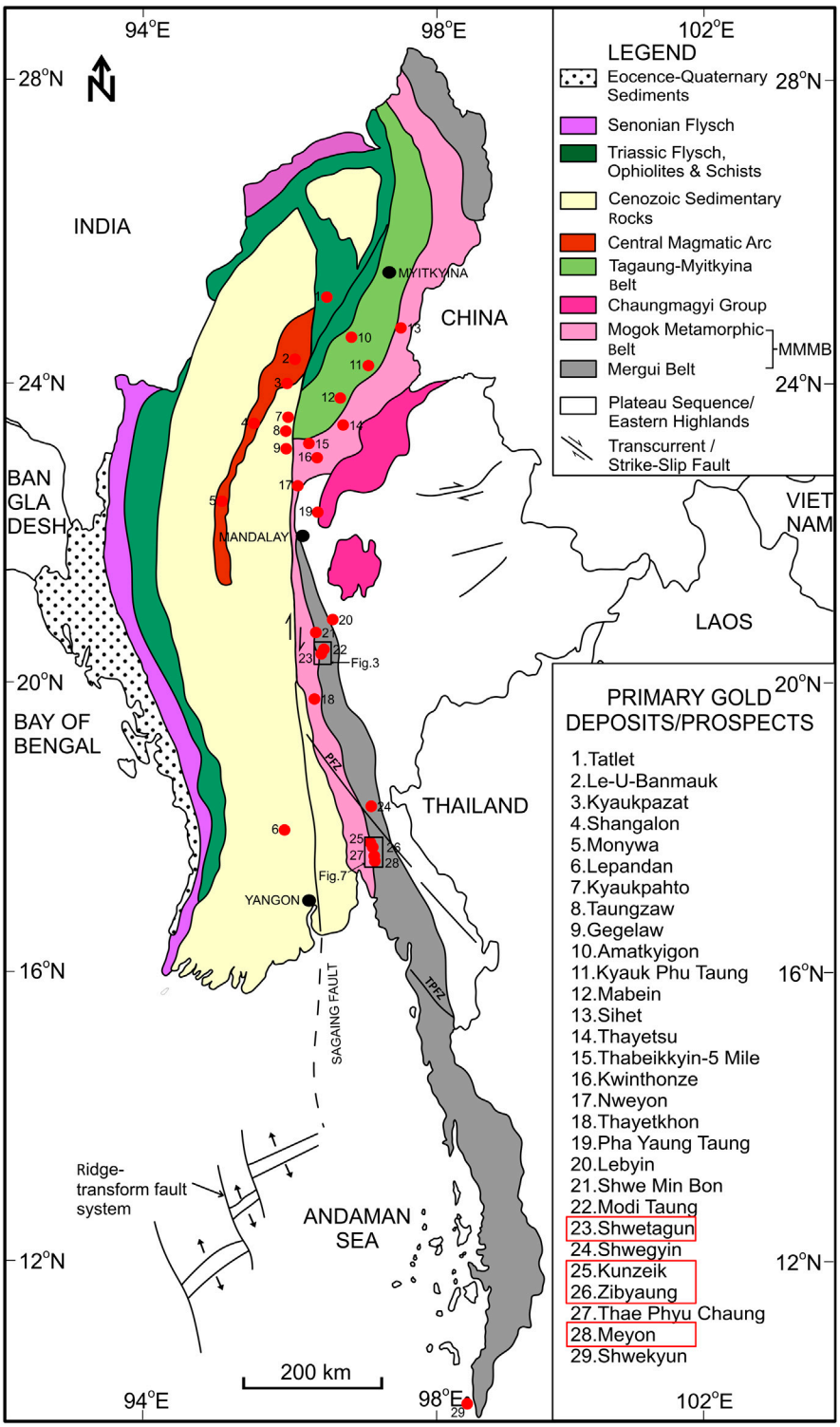

FIGURE 1 | Major structural belts, and gold occurrences in Myanmar (Modified after Mitchell et al., 2004; Ye Min Swe et al., 2017; Myo Kyaw Hlaing et al., 2019), PFZ, Papun Fault Zone; TPFZ, Three Pagodas Pass Fault Zone; MMMB, Mogok-Mandalay-Mergui Belt.

300 km long in the west of the Gaoligong Range in southern China (**Figures 1**, **2**; Mitchell et al., 2004, 2012; Gardiner et al., 2015, 2018; Mitchell, 2018).

The Mogok Metamorphic Belt (MMB) is described as the northern part of the MMMB (**Figures 1**, **2**). Although the local linkages between the MMB and the MB remain an open question

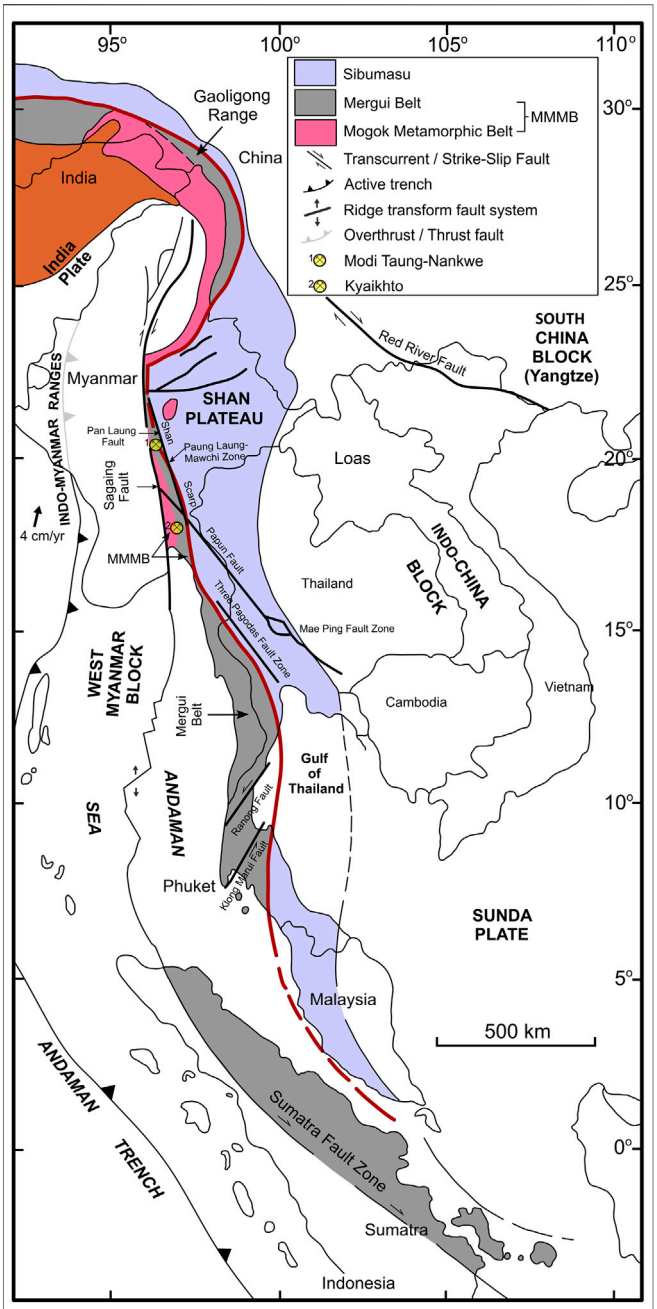

FIGURE 2 | Regional tectonic setting of Myanmar and distribution of Mergui Belt (Gaoligong Range and its southeastward continuation through Thailand into Indonesia). Red line at eastern margin of Mergui Belt is the Medial Myanmar suture zone (Modified after Mitchell, 2018). MMMB, Mogok-Mandalay-Mergui Belt.

(Gardiner et al., 2015), they defined the MB as the southern part of the MMMB. In MMMB, the granites are found in the east of the Sagaing Fault and at the west of the Panlaung-Mawchi Zone, which was located west of the Shan scarps (**Figures 2**, **3**). The MB is bordered on the west by schists, gneisses, marbles, and granites of the MMB (Chhibber, 1934), which are intruded by calc-alkaline dykes and granites (Mitchell et al., 2004). The MB is located along the north-trending zone related to the suturing of the Shan Plateau as part of the Sibumasu (a fragment of Gondwana) and the West Myanmar block, and between the Indo-Myanmar Ranges to the east and the South China block to the south and the Indochina block to the east (**Figures 1**, **2**). The MB consists of several NE-/W-trending faults which are formed within the central to the southern part of Myanmar and are notable for the existence of a large number of orogenic-style gold deposits (**Figures 1**, **2**). Most of the important gold deposits in the MB are associated with the second-order fault, N to NW trending upright folds, 1–6 km long, ductile shear zones, and are best referred to as orogenic gold deposits (e.g., Mitchell et al., 2004). The eastern boundary of the Shwetagun gold deposit in the MB is bordered by the Pan Laung fault, and the eastern margin is represented by the Paung Laung-Mawchi Zone (Shan Scarps) and the strata are dipping steeply to the west from the east of Nankwe to the Sakhanya Taung fault (**Figures 2**, **3**; Mitchell et al., 2004).

The Upper Jurassic rocks of the Paunglaung-Mawchi Zone are overthrusted by the Pan Laung fault along their western margins. The Papun fault lies in the south of the Modi Taung-Nankwe gold district in the MB and MMB, and at the west of the Paunglaung-Mawchi Zone (**Figures 2**, **3**). Gold occurrences in the Kyaikhto area occur close to the NNW–SSE striking Papun fault in the north and the Three Pagodas fault in the south. The Three Pagodas fault is almost parallel to the Papun fault and continuous from the Papun area to the southeast into Thailand, where it is regionally known as the Mae Ping fault or the Wang Chao fault (**Figure 2**; Ridd and Watkinson, 2013). The MB is considered to have formed as a complex fold and thrust belt with the Lower Cretaceous to Middle Miocene of Neo-Tethys accretionary wedge involving major sheared zones (Zaw Naing Oo and Khin Zaw, 2009, 2015, 2017; Khin Zaw et al., 2014a, 2017; Gardiner et al., 2016, 2018). This belt has been reactivated throughout the eastward subduction of continental blocks derived from the India-Asia collision zone to the north and lies north of the active subduction zone of the Sunda-Andaman arc (Mitchell et al., 2004, Zaw Naing Oo et al., 2010; Zaw Naing Oo and Khin Zaw, 2009, 2015, 2017; Khin Zaw et al., 2014a, 2017; Gardiner et al., 2016, 2018).

The MB is originally referred to as the Lower Jurassic regional metamorphic belt of major east-convergence origin that hosts several orogenic gold occurrences (Mitchell et al., 2004, 2012). The gold deposits within the MB are commonly associated with supracrustal rocks or in the vicinity of regional, crustal-scale deformation zones with a brittle to ductile type of deformation (e.g., Mitchell et al., 2004; Mitchell, 2018). The metasedimentary rocks within this belt are intruded by the granitoids of Central Granitoid Belt of Myanmar (or) Western Granite Province of Southeast Asia (**Figures 1**, **2**; Mitchell, 1977; Khin Zaw, 1990; Cobbing et al., 1992; Mitchell et al., 2004, 2012). The MB was also intruded by several generations of granitoid comprising numerous I-type and S-type two-mica granites of Cretaceous-Paleogene age (Khin Zaw, 1990; Cobbing et al., 1992; Barley et al., 2003; Searle et al., 2007; Mitchell et al., 2012; Gardiner et al., 2015, 2018; Aung Zaw Myint et al., 2017). The S-type granites are associated with significant tin-tungsten mineralization (Khin Zaw, 1990, 2017; Gardiner et al., 2014; Aung Zaw Myint et al., 2017; Mitchell, 2018). However, there is no geological evidence of preferential relationships of orogenic-type gold deposits with the

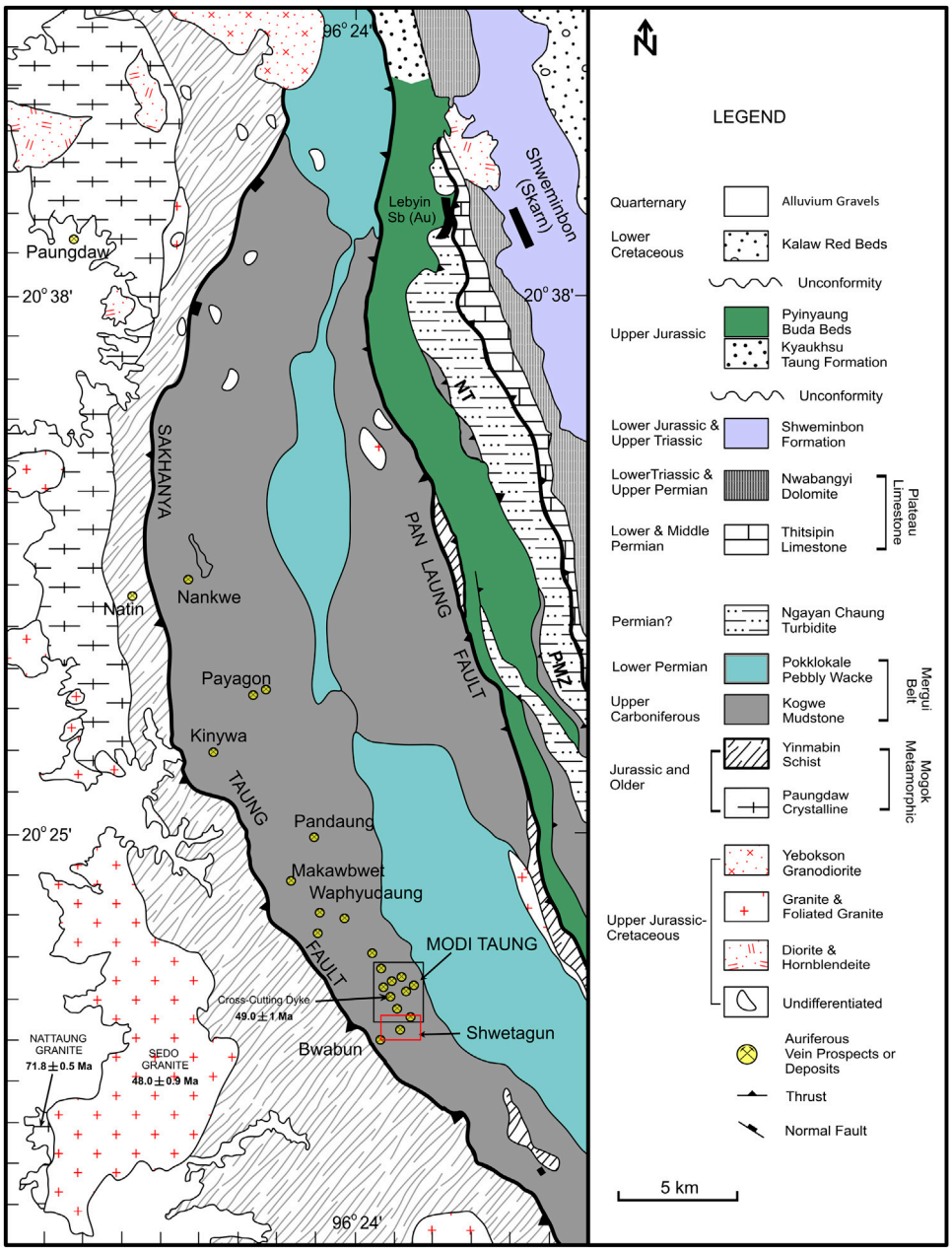

FIGURE 3 | Geological map of the Modi Taung-Nankwe gold district (Modified after Mitchell et al., 2004). NT, Ngapyaw Chaung Thrust; PMZ, Panlaung-Mawchi Zone.

Cretaceous-Eocene granite intrusions (Mitchell et al., 1999, 2004; Gardiner et al., 2014; Mitchell, 2018).

THE GEOLOGY OF GOLD DISTRICTS

Numerous orogenic gold deposits have been discovered in the MB. The Modi Taung-Nankwe and Kyaikhto gold districts lie within the MB from central to southern Myanmar (**Figures 2**, **3**). The geology of the Shwetagun deposit in the southwestern part of the Modi Taung-Nankwe gold district and the Kyaikhto gold district are described below.

Shwetagun Gold Deposit in Modi Taung-Nankwe Gold District

The gold mineralization of the Shwetagun deposit is located about 3 km south of the Modi Taung deposit (**Figures 3**, **4**). The Kogwe mudstone and Poklokkale Pebbly wackestone are mainly exposed at the Shwetagun area (Mitchell et al., 2004; Myo Kyaw Hlaing,

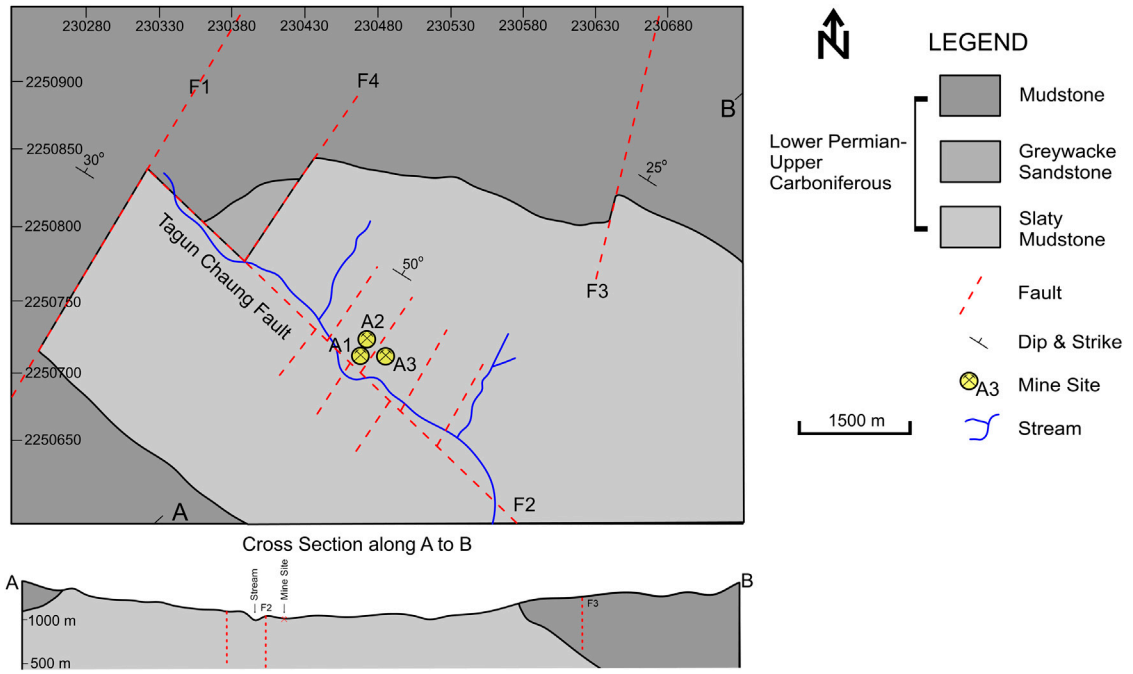

FIGURE 4 | Geological map of the Shwetagun gold deposit, Modi Taung-Nankwe gold district, Myanmar. Abbreviations: A1 = adit-I, A2 = adit-II, A3 = adit-III.

2013; Mitchell, 2018) and the gold mineralized veins are hosted by the Kogwe Mudstone Unit which consists of pebbly mudstone, siltstone and sandstone (Mitchell et al., 2004). Gold-quartz veins are oriented in NE-SW and N-S directions and can be grouped into one of the three vein systems within exploration Adit I, II and III (**Figures 4**, **5A–C**). The Adit I and II are located along the NE-SW strike, whereas Adit III trends north-south. Each vein system consists of either a single vein or multiple parallel veins separated by host rocks. Quartz veins in Adits I and II show stylolitic lamination and sheeted structure (**Figures 5A–C**) which indicate the movement on the shear planes during the formation of gold veins (e.g., Mitchell et al., 2004).

In Adit III, the strong post-vein faulting more or less along the plane of the shear resulted in pinched and swelled structure, and brecciation. F1 and F2 faults are mainly related to the mineralized veins where bedding is usually low angle with southeast-northwest trending fold axes; most veins intersect bedding at a high angle, cut crenulation cleavage where visible, cut the bedding plane, and accompanied by pervasive silicification of the mudstone (**Figures 5A–C**). The general trend of bedding is NE-SW direction paralleling the mineralized veins (**Figure 4**). En-echelon sigmoidal tension gashes filled with barren to weakly auriferous fibrous quartz are widespread in the mudstone sometimes kilometers away from the mineralized veins (**Figures 6A–D**). The tension gash veins in the shear zone imply ductile deformation which is evident for later faulting (**Figure 6C**). The Shwetagun area is structurally complex; there have been at least two or three deformation phases in both small-scale and major structures (e.g., Michell et al., 2004). No igneous rocks have been found at the Shwetagun area, and the nearest igneous rocks to the Modi Taung deposit are the microgranite porphyry at Theingi vein and the late dacite and andesite porphyry dykes which cut across the ore zone at Shwesin vein (Traynor et al., 2015, 2017) and Momi Taung, approximately 3 km northeast of Shwetagun (**Figure 3**).

Kyaikhto Gold District

The Kyaikhto gold district in the southern part of MB consists of several gold deposits and occurrences, including Kunzeik, Zibyaung and Meyon (**Figure 7**). The Kyaikhto gold occurrences are formed as sheeted veins, massive veins, network veinlets, stockworks, and disseminations. The structural setting at the Kyaikhto gold occurrences is dominated by NNE-SSW, and NW-SE striking faults (**Figure 7**). Mineralization in the Kyaikhto gold district is hosted by metasedimentary rocks of sandstone, slate, phyllite, and schist, and associated with the biotite granite and biotite granodiorite (**Figure 7**). The granitic rocks in this area can be correlated to the Mokpalin quartz diorite and the Kyaikhtiyo granite that have yielded the LA-ICP-MS zircon U-Pb ages of 90.8 ± 0.8 Ma and 63.3 ± 0.6 Ma, respectively (**Figure 7**; Mitchell et al., 2012; Myo Kyaw Hlaing et al., 2019). The metamorphic grade of the metasedimentary rocks is greenschist facies, characterized by a mineral assemblage of epidote, biotite, muscovite, and chlorite. Locally, fine-grained pyrite crystals are disseminated in the slate, phyllite, and schist (Myo Kyaw Hlaing et al., 2019).

The quartz vein systems almost invariably appear to be related to regional NNW -SSE trending structures which are commonly recorded along the MB (**Figure 2**). Brecciation and fracturing of the quartz vein contributed favorable sites for supergene gold enrichment processes (Zaw Naing Oo and Khin

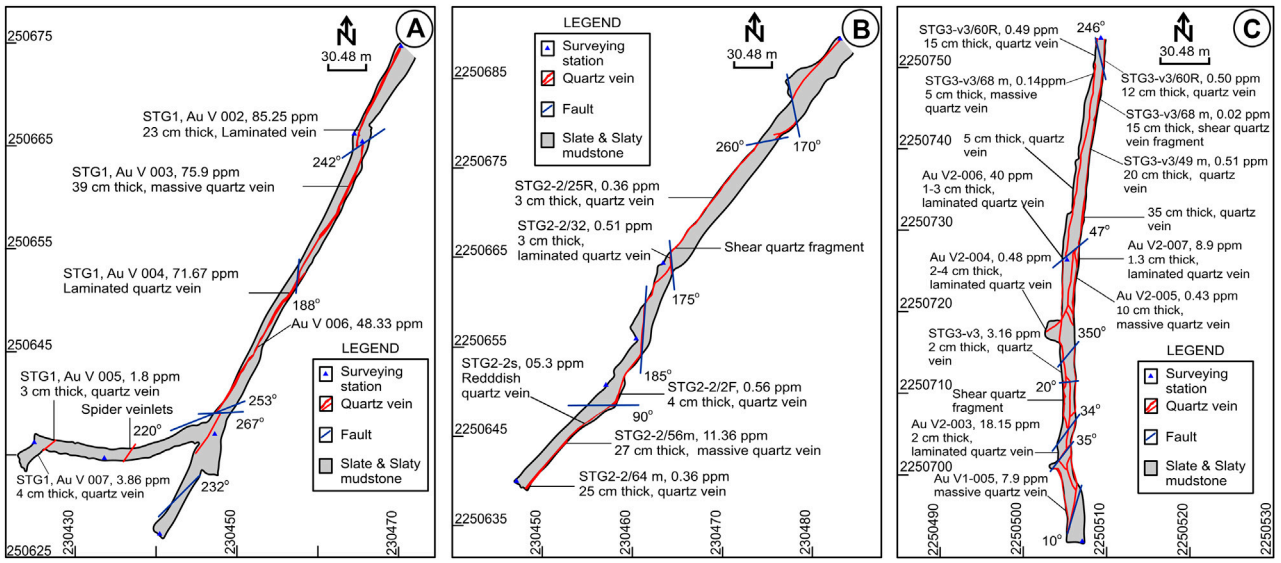

FIGURE 5 | (A) Mineralization map of the adit-I, **(B)** adit-II and **(C)** adit-III at Shwetagun, Modi Taung-Nankwe gold district, Myanmar.

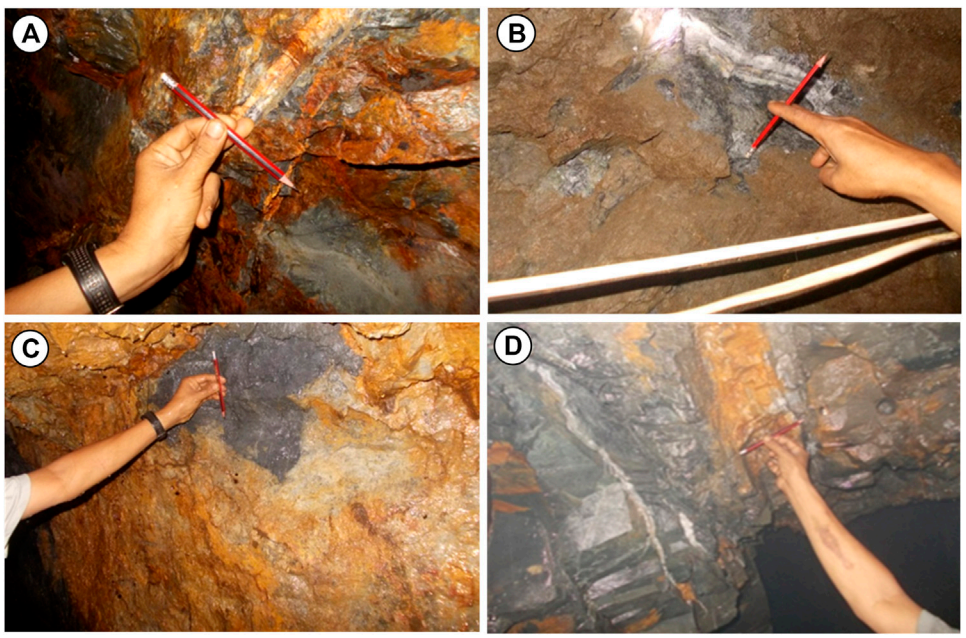

FIGURE 6 | Vein style and texture of the Shwetagun gold deposit. **(A)** Photographs showing auriferous sheeted quartz vein about 10 cm thickness at adit I, **(B)** auriferous sheeted quartz vein about 20 cm thickness at adit I, **(C)** distorted vein by the effects of shear force at adit II and **(D)** nature of auriferous sheeted quartz vein at adit III.

Zaw, 2009; Zaw Naing Oo et al, 2010; Zaw Naing Oo and Khin Zaw, 2015; 2017). The thickness of the tension gash veins and stockwork veins varies from a few 20 cm to 2 m wide. All of these gold deposits feature extensive, steeply dipping, vein systems, usually with multiple stages of vein development. In some deposits, the veins are slightly narrow (1–2 m) and separated, and there may be several parallel veins set within broad structural zones (e.g., Meyon). In other areas, such as at Kunzeik, the multiple vein systems form stockwork structures. At Zibyaung, the mineralized quartz veins are found as white to milky quartz. Mineralization in the Kyaikhto gold district is dominantly related to the deformation of the host rocks and occurred within structurally-controlled dilatant fractures.

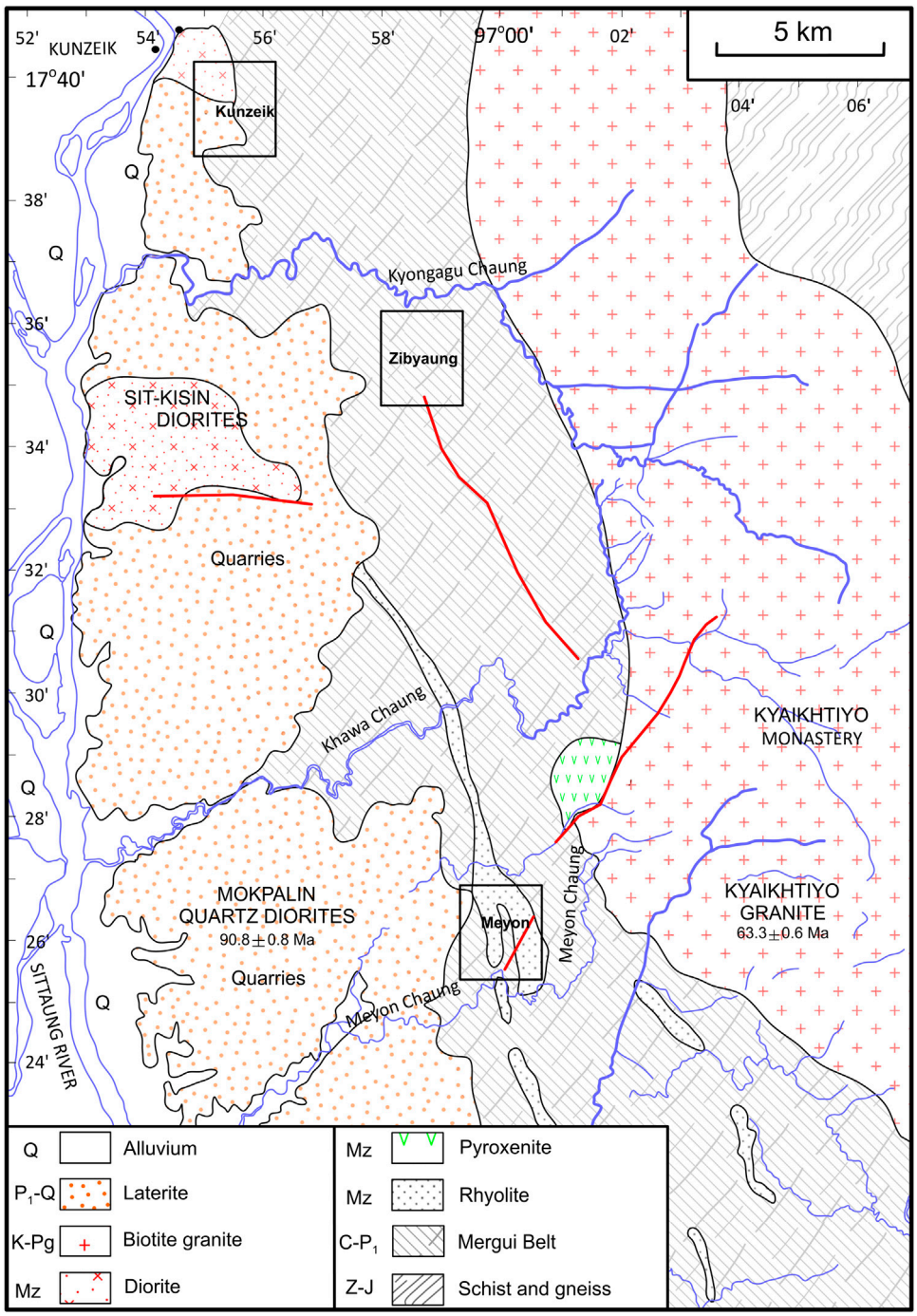

FIGURE 7 | Geological map of the Kyaikhto gold district. Red lines are faults (Modified after Mackenzie et al., 1999; Mitchell et al., 2012; Myo Kyaw Hlaing et al., 2019). Abbreviations: Q = Quaternary, P_1-Q = Lower Pliocene to Quaternary, K-Pg = Cretaceous to Paleogene, Mz = Mesozoic, C-P_1 = Upper Carboniferous to Lower Permian, ZJ = Late Proterozoic to partly Jurassic.

MATERIALS AND ANALYTICAL METHODS

During the years 2012–2018, representative samples of the Shwetagun deposit in the Modi Taung-Nankwe gold district and Kyaikhto gold district were collected from active mining operations. Forty samples were examined using a Rigaku Ultima IV X-ray diffractometer to detect alteration minerals, running at 40 kV and 20 mA with a CuKα varying from 2.0 to 65.0 (2θ).

Forty-five thin sections and seventeen polished sections were prepared for the examination of ore and gangue minerals from

the Shwetagun deposit and Kyaikhto gold occurrences using NIKON ECLIPSE LV100N POL petrographic microscope and the scanning electron microscope (SEM) with energy-dispersive X-ray spectroscopy (EDS) of HITACHI-SU3500 at the Center of Advanced Instrumental Analysis, Kyushu University. SEM-EDS analysis was used to determine the elemental composition of pyrite, chalcopyrite, sphalerite, arsenopyrite, galena, hematite, and other ore minerals, including the Au-Ag ratio of electrum.

Fifteen doubly polished thin sections of mineralized quartz were prepared from the Shwetagun deposit and Kyaikhto gold occurrences for fluid inclusion studies. Microthermometric measurements were conducted at Kyushu University using a Linkam-THMS600 heating-freezing stage equipped on a NIKON ECLIPSE LV100N POL petrographic microscope. The heating/freezing rate was generally 0.2–5.0°C/min but was <0.2°C/min near a phase transition. The uncertainties for the measurements are ±0.5, ±0.2 and ±2.0°C for runs in the range of −120 to −70°C, −70–100°C, and 100–600°C, respectively. The fluid inclusions were classified by the criteria of Roedder (1984). Total salinities of NaCl-H_2O inclusions were calculated from the final melting temperatures of ice using the equation by Bodnar (1993). Salinities of the inclusions of the CO_2-bearing fluid were computed using the melting temperatures of clathrate (Collins, 1979).

RESULTS

Hydrothermal Alteration

Shwetagun Gold Deposit in Modi Taung-Nankwe Gold District

The Shwetagun area comprises several zones of alteration, which occurred in structurally-controlled setting and the general trend is from NS to NE-SW. Two types of hydrothermal alterations are recognized: 1) a regional smectite/illite–chlorite–quartz alteration associated with silicified and slaty mudstone (**Figures 8A–C**); 2) chlorite-sericite-quartz–pyrite alteration associated with gold-quartz veins (**Figures 8A–C**). Chlorite-sericite-quartz–pyrite alteration forms on both sides of the ore veins (**Figures 8A–C**). Petrographic studies and XRD results of alteration mineral assemblages are described schematically in **Table 1**. The smectite/illite–chlorite–quartz alteration zone is dominated by laminated quartz veins with alternating quartz and chlorite-rich layers (**Figures 8A–C**). Smectite/illite–chlorite–quartz alteration forms as the outer zone of chlorite-sericite-quartz–pyrite alteration. The study area is also affected by supergene processes. The chlorite-sericite-quartz–pyrite alteration is overprinted by the secondary minerals (e.g., hematite) that were produced by oxidation process. The three most important hydrothermal alteration processes are silicification, chloritization, and sericitization (**Figures 8B–D**). Silicification occurs as fracture-controlled quartz veins and dense banding and irregular deformation-controlled lenses (**Figure 8D**). The most common alteration process is chloritization, which occurs around gold-bearing quartz veins (**Figure 8C**). There is an orthogonal setting between the intensity of brittle and ductile deformation and the degree of hydrothermal alteration (**Figure 8B**).

Kyaikhto Gold District

The quartz-gold veins in the Kyaikhto gold district are hosted within an intensely deformed sedimentary sequence comprising sandstone and carbonaceous mudstones (Myo Kyaw Hlaing et al., 2019). The host mudstone and phyllite are silicified and hydrothermally altered to assemblages with sericite, chlorite, kaolinite, and pyrite (Myo Kyaw Hlaing et al., 2019). At Kunzeik, the strongly altered rocks adjacent to the auriferous quartz veins are typically enriched in sulfide minerals (e.g., pyrite and chalcopyrite). Silicification and pyritization are easily observable close to the veins. Silicification was followed by sericitization in the felsic host rocks. At Zibyaung, the host phyllite is affected by an earlier (chlorite) alteration and later silicification and sericitization. Chloritization overprinting sericitization becomes more pervasive proximal to the distal parts of ore bodies. At Meyon, hydrothermal alterations are characterized by silicification and chloritization, sericitization, carbonate alteration, kaolinite, and albitic alteration and quartz infill of the metasedimentary rocks and ore breccias are also recorded. Sulfides are sparsely disseminated in the rock and completely altered to limonite (Zaw Naing Oo et al., 2010; Zaw Naing Oo and Khin Zaw, 2015, 2017).

Ore Mineralogy

Microscopically, the ore samples show various mineral assemblages and indications of fracture fillings as well as replacement textures. Based on microscopic observation, there are two types of gold-bearing sulfide ore textures: the disseminated and fracture-filling sulfide types (**Figures 9A,B,D,E**). The electrum occurs as submicron-sized inclusions in the fracture of sulfides at Shwetagun (**Figures 9A,B**). Most of the electrum grains are identified as free grains, but some are intergrown with pyrite, chalcopyrite, galena and sphalerite. Locally, it is concentrated as clumps of irregular electrum grains dispersed in alteration minerals. Some electrum grains are lighter and gradually change to whitish color with very high reflectivity, due to presence of high silver content. The electrum grains at Shwetagun yielded an Au content of 72.9–74.3 atomic %. Sphalerite is one of the major ore minerals and appears in euhedral to subhedral aggregates up to 5 mm in size (**Figure 9C**). The FeS mol% of sphalerite is between 4.02 and 8.41. Chalcopyrite is a primary important hypogene mineral in the ore textures (**Figure 9E**).

Pyrite is the most abundant sulfide mineral at Shwetagun. It occurs as fine-grained, massive aggregate and euhedral to subhedral crystals along the outer margin of the quartz veinlets. The earliest sulfide mineral is invariably pyrite, with deeply fractured sub-euhedral crystals that are locally replaced by other base-metal sulfides (**Figures 9A–E**). A few grains of pyrite are replaced by chalcopyrite along their grain boundaries and microfractures (**Figure 9E**).

At Kunzeik, the quartz-carbonate-sulfide vein consists of chloritized host rock fragments surrounded by irregular to massive aggregates of pyrite, chalcopyrite, and sphalerite

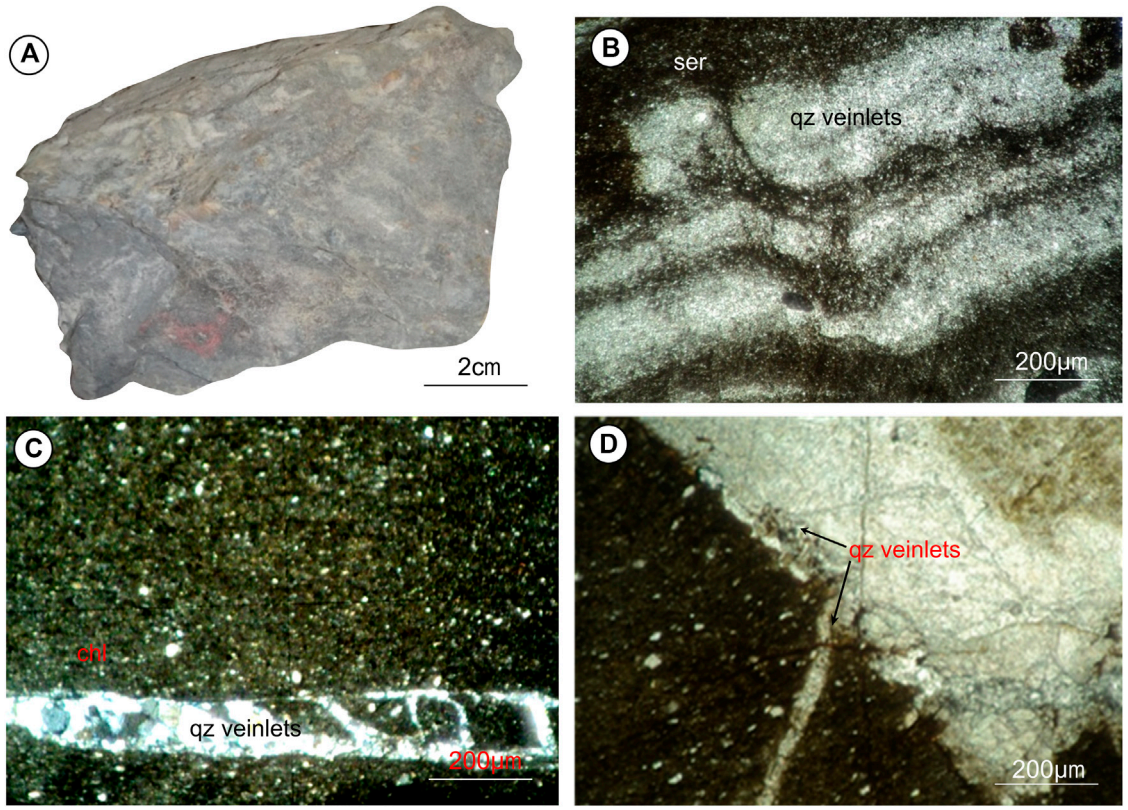

FIGURE 8 | Lithology and microscopic vein texture of the Shwetagun gold deposit. **(A)** Photographs showing slaty mudstone host rock in shear zone from adit I, **(B)** Photomicrographs showing ductile structures with sericite alterations in slaty mudstone from adit II, **(C)** chlorite alterations from adit II and **(D)** Silicification from adit I. Abbreviations: qz = quartz ser = sericite and chl = chlorite.

TABLE 1 | Summary of hydrothermal alteration from orientated samples analyzed by XRD and microscopy.

Deposit Name	Sample No	Rock Name	Kaolinite	Smectite/illite	Sericite	Chlorite	Pyrite
Shwetagun	STG03 (adit-I)	Silicified Mudstone	++	+++	—	+++	—
	STG07 (adit-I)	Greywacke	++	+++	—	+++	—
	STG09 (adit-II)	Slaty Mudstone	++	+++	++	+++	—
	STG10 (adit-II)	Slaty Mudstone	++	+++	—	+++	—
	STG14 (adit-III)	Slate	++	+++	+++	+++	+
Kunzeik	KZ04	Slate	++	+++	+++	++	+
	KZ05	Slate	++	+++	+++	+++	+
Zibyaung	ZB06	Slaty phyllite	++	+++	+++	++	+
	ZB07	Slaty phyllite	++	+++	+++	+	+

Notes: +++ Common, ++ Few, + Rare, - Not Detected.

together with quartz and chlorite (**Figure 9F**; Myo Kyaw Hlaing et al., 2019). Electrum, sphalerite, and galena are mostly found in pyrite at Zibyaung (**Figures 9G,H**; Myo Kyaw Hlaing et al., 2019). Sphalerite forms as a fissure filling mineral within pyrite. Galena occurs as fine-to medium-sized grains filling cracks in pyrite and sphalerite. Electrum grains with an atomic % of 74.5–78.1 Au can be detected as minute grains in pyrite with galena, and sphalerite (**Figure 9F–H**). The FeS mol% of sphalerite ranges from 4.98 to 7.26. At Meyon, chalcopyrite is associated with pyrite and covellite. Covellite occurs as a secondary replacement mineral of chalcopyrite (Myo Kyaw Hlaing et al., 2019). Native gold also develops as free grains in the oxidized zone and fracture fillings within pyrite. Pyrite occurs as two generations, idiomorphic grains intergrown with chlorite aggregates or in contact with massive chalcopyrite, pyrrhotite, arsenopyrite, marcasite, magnetite and hematite (Zaw Naing Oo and Khin Zaw, 2009; Zaw Naing Oo et al, 2010; Zaw Naing Oo and Khin Zaw, 2015; 2017; Myo Kyaw Hlaing et al., 2019).

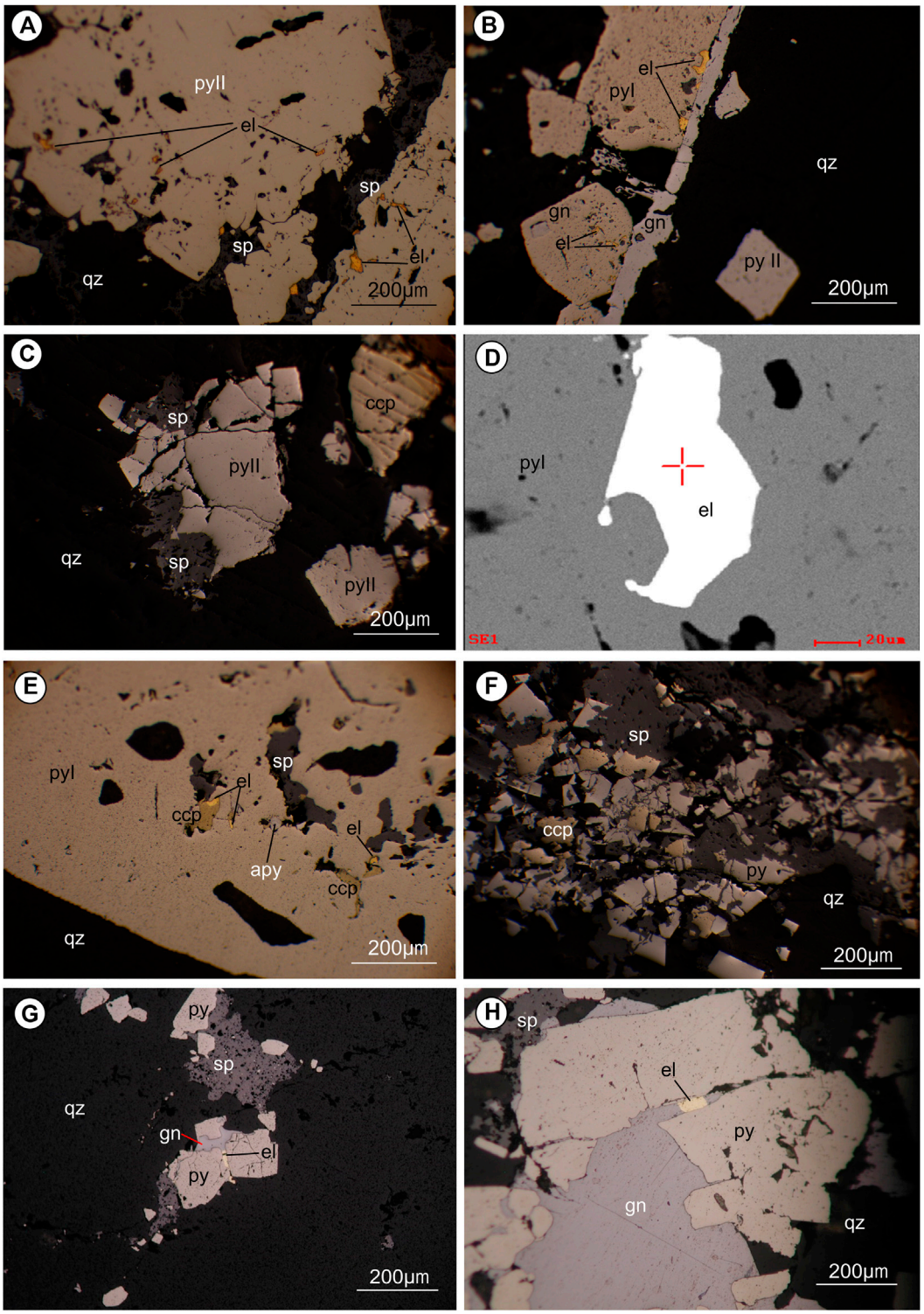

FIGURE 9 | Photomicrographs showing **(A)** electrum inclusion in subhedral pyrite (py II) with sphalerite of the gold-bearing quartz vein in adit-I from Shwetagun, **(B)** fractured electrum filled with euhedral pyrite (py I) and galena, suggesting their chronological relationship of the gold-bearing quartz vein in adit I from Shwetagun, **(C)** euhedral pyrite (py I) associated with sphalerite and chalcopyrite of the gold-bearing quartz vein in adit-III from Shwetagun, **(D)** backscattered electron image with an electrum grain in pyrite from Shwetagun, **(E)** electrum inclusion is surrounded by chalcopyrite, sphalerite and arsenopyrite in pyrite from Shwetagun, **(F)** massive pyrite aggregates with chalcopyrite, and sphalerite of quartz-carbonate-sulfide vein from the Kunzeik, **(G)** and **(H)** fractured electrum filled with euhedral pyrite, galena and sphalerite of quartz-sulfide vein from Zibyaung. Figures (g) and (h) are taken from Myo Kyaw Hlaing et al. (2019). Abbreviations: py = pyrite, gn = galena, ccp = chalcopyrite, sp = sphalerite, apy = arsenopyrite, el = electrum and qz = quartz.

Fluid Inclusion Characteristics

Fluid inclusions studies have been performed in quartz, quartz-sulfide and quartz-carbonate-sulfide veins from the Shwetagun, Kunzeik and Zibyaung deposits (**Figures 10A–D**). At Shwetagun, fluid inclusions were found in quartz in the mineralized veins quartz. There are two types of fluid inclusions: Type A (vapor-rich) and Type B (liquid-rich). Type A (vapor-rich) and Type B (liquid-rich) aqueous fluid inclusions were observed in all quartz samples and occur as isolated groups of primary inclusions as clusters and pseudo-secondary trails. Secondary fluid inclusions (trail-bound) are also present but are extremely small (<2 μm) and have not been studied. Most fluid inclusions were aqueous (H_2O) fluid inclusions. At Kunzeik and Zibyaung, two types of fluid inclusions were found in quartz and calcite of quartz-carbonate-sulfide and quartz-sulfide veins at room temperature (**Figures 11A–H**). Based on the criteria described by Roedder (1984), the fluid inclusions were classified as primary, pseudo-secondary, and secondary, and given below: Type A (aqueous-carbonic) inclusions, Type B (aqueous) inclusions.

Type A (*aqueous-carbonic inclusions*): This type belongs to the H_2O–CO_2–NaCl system and occur in quartz and calcite of the mineralized vein quartz. They are 5–10 μm in size and have bi-phase (liquid and vapor) at room temperature. These inclusions also show presence of three phase (liquid H_2O, liquid CO_2, vapor CO_2) and clathrate during freezing runs. The CO_2: H_2O ratio in these inclusions range from 80: 20 to 50: 20. Occasionally vapor bubbles are moving but no liquid CO_2 is present (**Figures 11C,E–G**).

Type B (*aqueous inclusions*): have been identified in quartz and calcite of the mineralized vein quartz. These inclusions are bi-phase with a vapor bubble and liquid at room temperature (**Figures 11C–F,H**).

Fluid Inclusion Microthermometry

Fluid inclusion characteristics of the gold deposits are summarized in **Table 2** and **Figures 12**, **13**. At Shwetagun, the final ice melting temperatures ($T_{m\text{-}ice}$) for Type A (vapor-rich) aqueous inclusions in quartz range from →0.1 to →2.8 (n = 10) (**Table 2**). The homogenization temperatures of Type A (vapor-rich) aqueous fluid inclusions in quartz of veins vary from 250 to 335 °C (n = 15), with salinities from 0.2 to 4.8 wt% NaCl equivalent (**Table 2**; **Figures 12A,B**). The final ice melting temperatures ($T_{m\text{-}ice}$) of Type B (liquid-rich) aqueous inclusions in quartz of veins studied range from -1.2 to -2.7 (n = 14). The homogenization temperatures of Type B (liquid-rich) aqueous fluid inclusions in quartz were from 261 to 320°C (n = 16), with salinities from 3.1 to 4.5 wt% NaCl equivalent (**Table 2**; **Figures 12A,B**).

At Kunzeik, complete homogenization temperatures (T_h) of (Type A) aqueous-carbonic fluid inclusions in quartz vary between 315°C and 356 °C (n = 21) (**Figure 12C**). Homogenization temperatures (T_h) of the (Type B) aqueous fluid inclusions in quartz of the mineralized vein quartz yielded a range approximately 246°C–376 °C (n = 21) (**Figure 12D**). The melting of CO_2 ($T_{m\ -CO2}$) in (Type A) aqueous-carbonic inclusions in quartz were between → 58.2°C and → 56.8°C (**Table 2**). The CO_2 phases of the (Type A) aqueous-carbonic inclusions in quartz were fully homogenized to the liquid phase at temperatures ($T_{h\text{-}CO2}$) of 25.5°C–30.9°C. The melting temperatures of clathrates in quartz ($T_{m\text{-}cla}$ = 7.6°C–9.2°C) (n = 10) suggest that the salinity of these inclusions is low, around 1.6 to 4.6 wt% NaCl equivalent. The final ice melting temperatures of (Type B) aqueous fluid inclusions in quartz range between → 0.6 and → 7.2°C (n = 14) corresponding to salinities between 1.1 and 10.7 wt% NaCl equivalent.

Total homogenization temperatures (T_h) of (Type A) aqueous-carbonic fluid inclusions in calcite range from 273°C to 318°C (n = 17) (**Figure 12C**). Homogenization temperatures (T_h) of the (Type B) aqueous fluid inclusions in calcite of the vein quartz yielded a range from 248°C to 325 °C (n = 20) (**Figure 12D**). The melting of CO_2 ($T_{m\ -CO2}$) in (Type A) aqueous-carbonic inclusions in calcite took place between → 57.2°C and → 56.8°C (**Table 2**). The CO_2 phases of the (Type A) aqueous-carbonic inclusions in calcite were completely homogenized to the liquid phase at temperatures ($T_{h\text{-}CO2}$) of 21.5°C–29.9°C. The melting temperatures of clathrates in calcite ($T_{m\text{-}cla}$ = 8.6°C–9.2°C) (n = 11) indicates that the salinity of these inclusions are generally low, about 1.6–2.8 wt% NaCl equivalent. The final ice melting temperatures of (Type B) aqueous fluid inclusions in calcite range from → 1.2°C to → 6.8°C (n = 13) corresponding to salinities from 2.1 to 10.2 wt% NaCl equivalent.

At Zibyaung, homogenization temperatures of the (Type A) aqueous-carbonic fluid inclusions in quartz of vein range between 312°C and 348°C (n = 19). The homogenization temperatures of (Type B) aqueous fluid inclusions in quartz of the vein vary between 242°C and 358°C (n = 19). The values of (Type A) aqueous-carbonic inclusions $T_{m\text{-}CO2}$ fall in the range of → 57.3 to → 56.8°C, indicating the only presence of pure CO_2. However, a few inclusions show $T_{m\text{-}CO2}$ values around -60°C, which can be due to the presence of minor other volatile components (Roedder, 1984). The first melting of ice ($T_{m\text{-}ice}$) in most of the (Type A) aqueous-carbonic fluid inclusions in quartz occurred between 20.5 and 30.9°C (n = 8) (**Table 2**). The temperatures of clathrate melting ($T_{m\text{-}cla}$) are between 4.6 and 9.6°C wt% NaCl equivalent (**Table 2**; **Figure 12E**). Final melting of ice ($T_{m\text{-}ice}$) in (Type B) aqueous fluid inclusions in quartz was observed in a temperature range from → 0.5 to → 8.1°C (n = 11) (**Table 2**), suggesting the salinities from 0.9 to 11.8 wt% NaCl equivalent (**Figure 12F**). Box and whisker plots of results from two and three phase fluid inclusions in the two gold districts are shown in **Figures 13A,B**.

DISCUSSION

Comparison With Orogenic Gold Deposits Worldwide

Several geological and geochemical characteristics of the MB gold deposits are comparable with those of the typical orogenic gold deposits worldwide (**Table 3**; e.g., Groves et al., 1998; Hagemann and Cassidy, 2000; Kerrich et al., 2000; Poulsen et al., 2000; Goldfarb et al., 2001; Robert and Poulsen, 2001; Groves et al., 2003; Goldfarb et al., 2005; Robert et al., 2005; Large et al., 2011; Groves et al., 2019). The gold deposits of the MB have a number

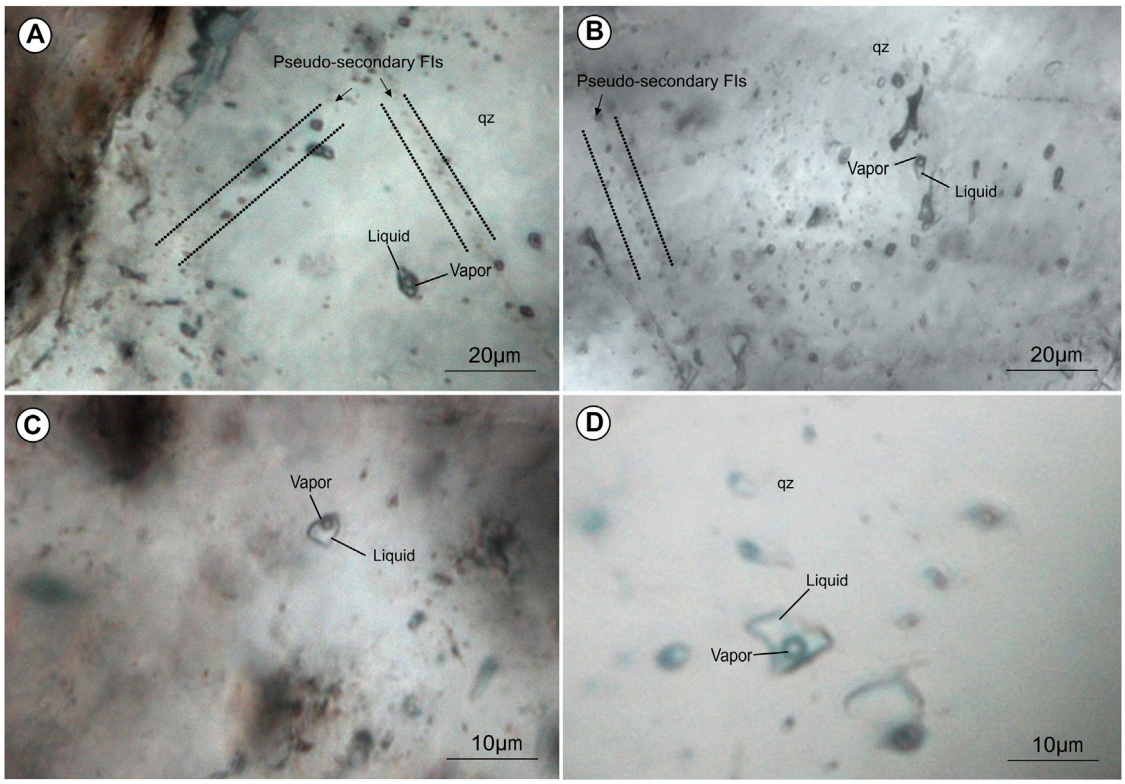

FIGURE 10 | (A) Photomicrographs of fluid inclusions in gold-bearing quartz vein from Shwetagun at room temperature in plane-polarized light. (a) and **(B)** Type A (vapor-rich) and Type B (liquid-rich) fluid inclusions coexisting together within same quartz gain in gold-bearing quartz vein from adit-I, **(C)** Type B (liquid-rich) fluid inclusions in quartz of the gold-bearing quartz vein from adit-I; and **(D)** Type B (liquid-rich) fluid inclusions in quartz of the gold-bearing quartz vein from adit-III. Abbreviations: qz = quartz.

of characteristics that are consistent with an orogenic gold system, including a close association between mineralization and deformation, and mineral assemblages of veins and alteration that are similar to Archean and Paleozoic gold systems (e.g., Groves et al., 1998; Bierlein and Crowe 2000; Hagemann and Cassidy 2000; Large et al., 2007). The orogenic gold systems are formed from the crustal fluids produced during the prograde metamorphism at the greenschist-amphibolite facies transformation and developed at intermediate depths (2–10 km) (Groves et al., 1998, 2003, 2020; Bierlein and Crowe, 2000; Goldfarb et al., 2001, 2005; Phillips and Evans, 2004; Dubé and Gosselin, 2007; Phillips and Powell, 2009, 2010; Tomkins, 2013; Goldfarb and Groves, 2015). Metamorphic fluids are generally regarded to be significant in the formation of orogenic gold deposits (e.g., Groves et al., 1998, 2003). There is still some debate over the appropriate source of orogenic gold ore fluids and the metals they transport (Tomkins, 2013; Goldfarb and Groves, 2015; Wyman et al., 2016; Groves et al., 2020). In comparison, Wyman et al. (2016) explored the presence of magmatic fluids in various orogenic gold deposits worldwide, as well as providing a comprehensive review of mineralizing fluids in orogenic gold systems. The formation of the widespread alteration of albite-silica-chlorite-sericite-carbonate-pyrite associated with the gold-bearing quartz veins in the MB was a major enhancing mineralizing mechanism for many other orogenic gold deposits worldwide (e.g., Phillips, 1993; McCuaig and Kerrich 1998; Goldfarb et al., 2005). The worldwide examples of these structural setting of the orogenic gold deposits are recorded at Golden Mile in Kalgoorlie, Western Australia, Western Lachlan Orogen in Victoria, SE Australia, Buller Terrane in western South Island, New Zealand, Meguma Terrane in Nova Scotia, Canada and Main Divide and Pingfengshan gold mine in Taiwan (**Table 3**; Shackleton et al., 2003; Bierlein et al., 2004; Groves et al., 1998, 2003; Goldfarb et al., 2001, 2005; Craw et al., 2010). Similar structural settings of the gold deposits are found in Myanmar at Phayaung Taung, Modi Taung and Shwegyin (**Table 3**; Mitchell et al., 2004; Win Phyo et al., 2016; May Thwe Aye et al., 2017; Ye Myint Swe et al., 2017).

Fluid Evolution and Depth Estimation

The microthermometric characteristics of fluid inclusions, alteration types, host rocks and tectonic setting related to various stages of vein formation of the mineralized quartz vein systems of Shwetagun (Modi Taung-Nankwe) and the Kyaikhto gold districts are remarkably similar. A majority of orogenic gold deposit studies have reported ore-mineralizing fluids to be of low salinity and aqueous-carbonic in composition (e.g., McCuaig and Kerrich 1998; Ridley and Diamond, 2000; Groves et al., 2003;

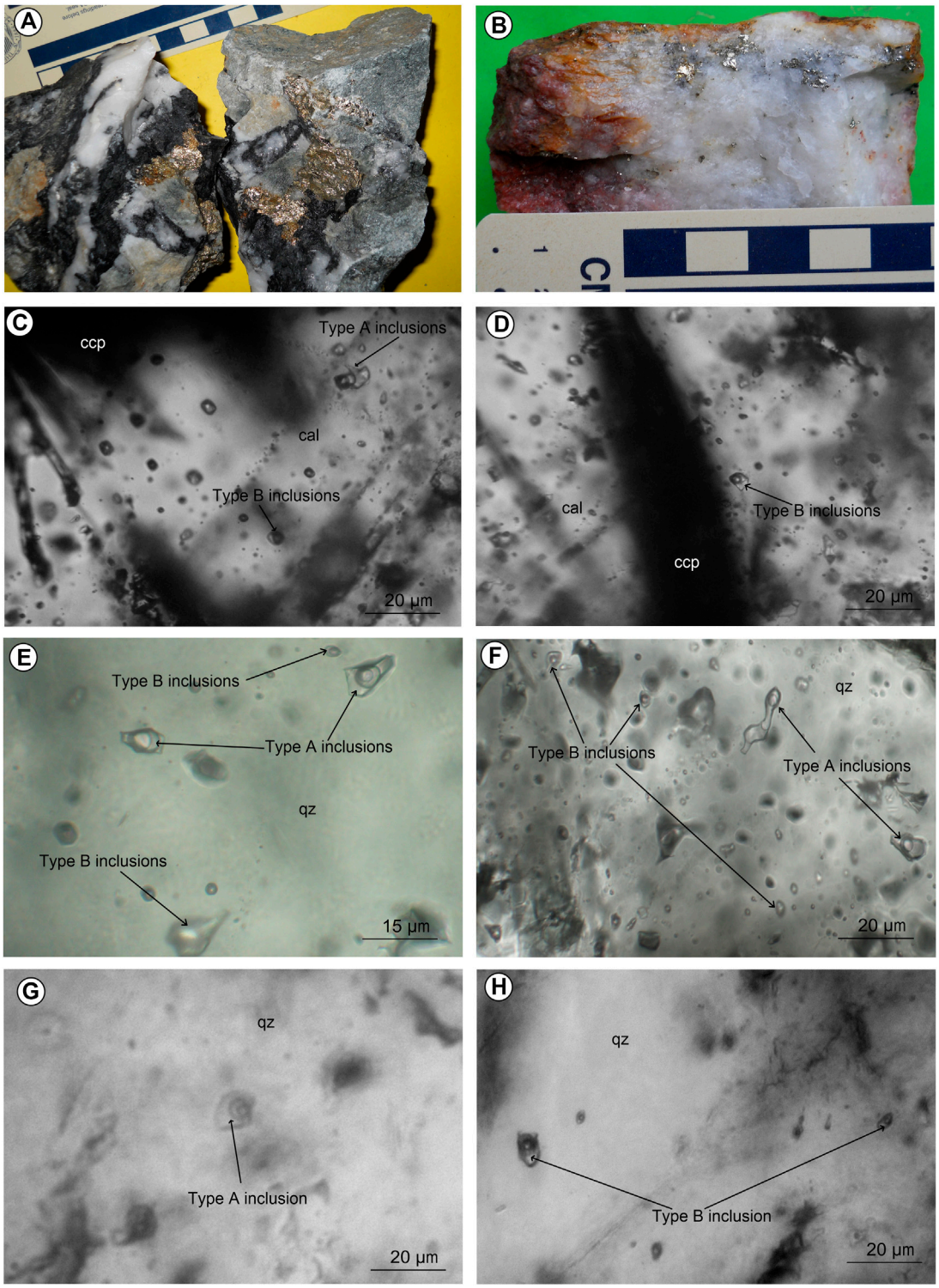

FIGURE 11 | Photographs showing the quartz veins of the deposits. **(A)** quartz-carbonate-sulfide vein from Kunzeik, **(B)** quartz-sulfide vein from Zibyaung, and photomicrographs **(C)** and **(D)** showing Type A (aqueous-carbonic) and Type B (aqueous) fluid inclusions in calcite of the quartz-carbonate-sulfide vein from Kunzeik, **(E)** and **(F)** showing Type A (aqueous-carbonic) and Type B (aqueous) fluid inclusions in quartz of the quartz-carbonate-sulfide vein from Kunzeik, **(G)** and **(H)** Type A (aqueous-carbonic) and Type B (aqueous) fluid inclusions in quartz of the quartz-sulfide vein from Zibyaung. Abbreviations: ccp = chalcopyrite, cal = calcite and qz = quartz.

TABLE 2 | Comparative analyses of fluid inclusion types and microthermometric results of the Shwetagun, Kunzeik and Zibyaung deposits.

Deposit Name	Vein Type	Type	$T_{m\text{-}CO2}$ (°C)	$T_{m\text{-}cla}$ (°C)	$T_{h\text{-}CO2}$ (°C)	T_h (°C)	$T_{m\text{-}ice}$ (°C)	Host mineral	Salinity (wt% NaCl eq.)	CO_2 density g/cm^3	Bulk density g/cm^3	References
Shwetagun	Gold quartz vein	Types A	—	—	—	250 to 335	−0.1 to −2.8	Quartz	0.2 to 4.6	—	0.62 to 0.83	This study
		Type B	—	—	—	261 to 320	−1.8 to−2.7		3.1 to 4.5	—	0.67 to 0.82	
Kunzeik	Quartz-carbonate -sulfide vein	Type A	−58.2 to −56.8	7.6 to 9.2	25.5 to 30.9	315 to 356	—	Quartz	1.6 to 4.6	0.53 to 0.70	—	Myo Kyaw Hlaing et al., 2019
		Type B	—	—	—	246 to 376	−0.6 to −7.2		1.1 to 10.7	—	0.53 to 0.89	This study
		Type A	-57.2 to -56.8	8.6 to 9.2	21.5 to 29.9	273 to 318	—	Calcite	1.6 to 2.8	0.61 to 0.75	—	
		Type B	—	—	—	248 to 325	−1.2 to −6.8		2.1 to 10.2	—	0.67 to 0.89	
Zibyaung	Quartz-sulfide vein	Type A	−57.3 to −56.8	4.6 to 7.6	20.5 to 30.9	312 to 348	—	Quartz	4.6 to 9.6	0.53 to 0.77	—	Myo Kyaw Hlaing et al., 2019
		Type B	—	—	—	242 to 358	−0.5 to −8.1		0.9 to 11.8	—	0.53 to 0.91	This study

Notes: $T_{m\text{-}CO2}$—melting temperature of CO_2; $T_{m\text{-}cla}$—melting temperature of CO_2 clathrate; $T_{h\text{-}CO2}$—partial homogenization temperature of CO_2 inclusions; T_h—total homogenization temperature of inclusions; $T_{m\text{-}ice}$—final ice melting temperature; wt% NaCl eq., weight percent NaCl equivalent.

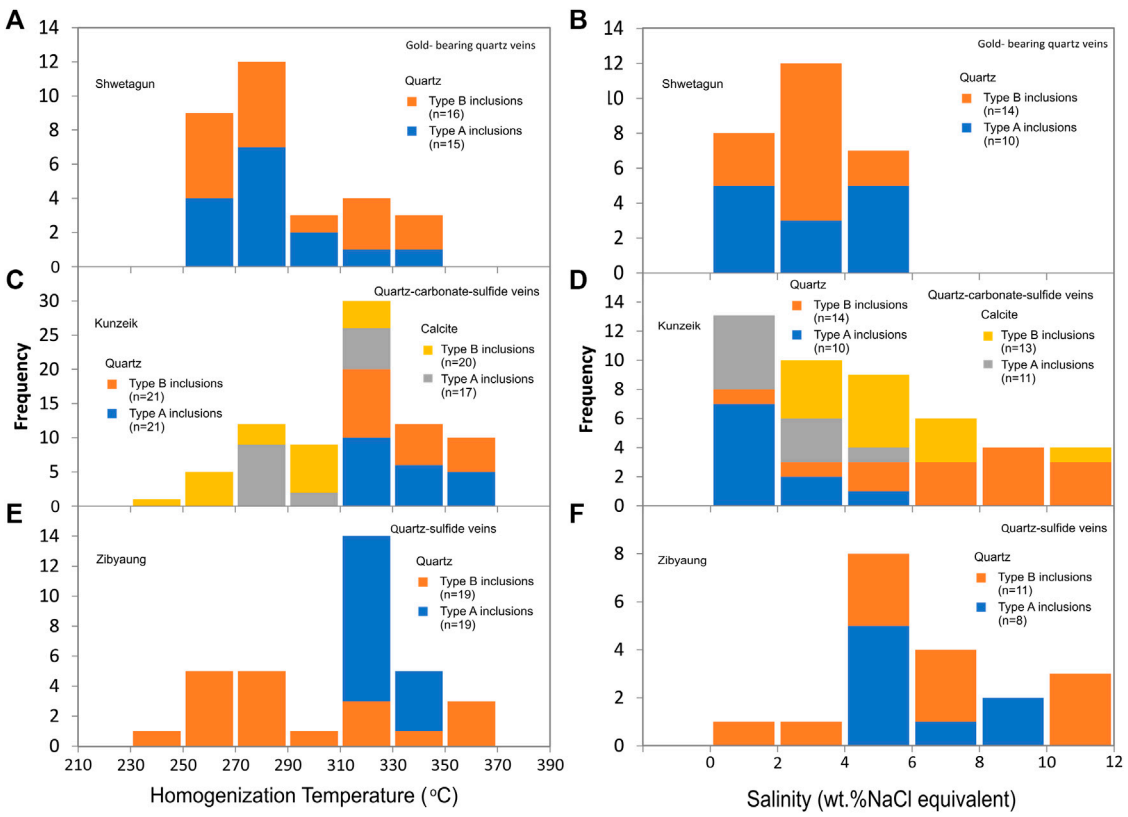

FIGURE 12 | Histograms of total homogenization temperatures (T_h) and salinities of primary fluid inclusions in quartz, quartz-sulfide and quartz-carbonate-sulfide veins from the deposits. **(A)** Histograms of T_h of primary fluid inclusions in gold-bearing quartz veins from the adit-I, II and III at Shwetagun, **(B)** Salinities of fluid inclusions in gold-bearing quartz veins from the adit-I, II and III at Shwetagun, **(C)** Histograms of T_h of primary fluid inclusions in quartz-carbonate-sulfide veins from Kunzeik, **(D)** Salinities of fluid inclusions in quartz-carbonate-sulfide veins from Kunzeik, **(E)** Histograms of T_h of primary fluid inclusions in quartz-sulfide veins from Zibyaung, and **(F)** Salinities of fluid inclusions in quartz-sulfide veins from Zibyaung. Figures **(C)**, **(D)**, **(E)** and **(F)** are adapted from Myo Kyaw Hlaing et al. (2019). Abbreviations: n = number of fluid inclusions.

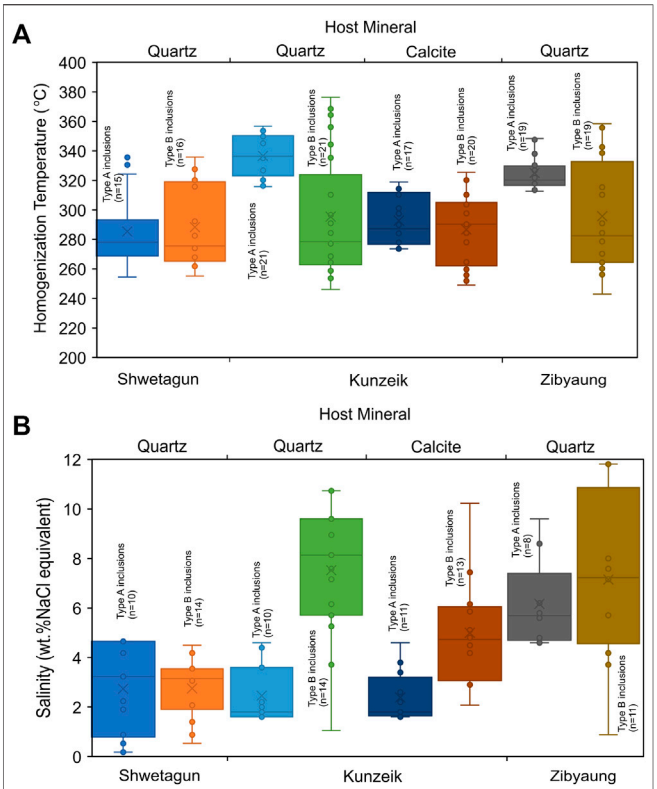

FIGURE 13 | Box and whisker plots showing **(A)** total homogenization temperatures and **(B)** calculated salinity values in two and three phase fluid inclusions from Shwetagun, Kunzeik, and Zibyaung. Abbreviations: n = number of fluid inclusions.

Goldfarb et al., 2005). The abundant aqueous fluid inclusions are similar to gold-related fluids throughout the belt, and typical of orogenic gold deposits elsewhere (e.g., Ridley and Diamond, 2000; Groves et al., 2003).

At Shwetagun, Type A (vapor-rich) inclusions are much less abundant than the Type B (liquid-rich) fluid inclusions, but they were observed as primary and pseudo-secondary inclusions in all samples. The secondary fluid inclusions have similar microthermometric properties to the primary inclusions, indicating that they represent events of vein reactivation in an evolving hydrothermal environment (Roedder, 1984). The ore fluid of Shwetagun ore-forming fluids evolved from a low to medium temperature (250–335°C), low salinity (0.2–4.6 wt% NaCl equivalent).

According to microthermometric results, a drop in salinities is found simultaneously with a decrease in temperature, suggesting that the system is diluted with cooling during the fluid evolution at Shwetagun. The major mechanism of ore and gangue mineral precipitation in veins is temperature drop (**Figure 14**). The absence of CO_2 in the gold-bearing veins at the Shwetagun deposit is in contrast to many ancient orogenic gold deposits, where separate phases of CO_2 are commonly found in fluid inclusions (Groves et al., 1998; McCuaig and Kerrich 1998; Bierlein and Crowe 2000; Goldfarb et al., 2004, 2005; Craw et al., 2010). However, the abundant CO_2 in the fluid is not a prerequisite for orogenic gold mineralization. (e.g., Main Divide and Pingfengshan gold mine in Taiwan; Craw et al., 2010 and references therein). The bulk densities of ore fluids from the Shwetagun deposit range from 0.62 to 0.83 g/cm^3 (**Table 2**). Although no depth estimation of the Shwetagun deposit is possible by fluid inclusion evidence, Mitchell et al. (2004) estimated a depth of 4–7 km based on stratigraphic and structural evidence.

In comparison, fluid inclusions in these deposits at Kunzeik and Zibyaung are dominated by earlier Type A (aqueous-carbonic) and Type B (aqueous) fluids. Histograms of homogenization temperatures and salinities, as well as a diagram of homogenization temperatures versus salinities, show a wide range of homogenization temperatures between 242 and 376°C, and low to medium salinities between 0.9 and 11.8 wt% NaCl equivalent, respectively (**Table 2**; **Figures 12–14**).

According to microthermometric results, the range of total homogenization temperatures (242–376°C) indicate that there may have been more than one episode of CO_2 phase separation during vein formation. The wide range of salinity also indicates a source of fluid, possibly mixed with low-salinity exotic fluid (**Figure 14**). Based on the relative timing of fluid inclusions, Type B (aqueous) fluids formed first, followed by Type A (aqueous-carbonic) fluids (**Figure 14**). The Kunzeik and Zibyaung fluids show two totally identical processes of total homogenization of Type A (aqueous-carbonic) and Type B (aqueous) inclusions within a similar temperature range, indicating that they were trapped together and may represent the same H_2O-CO_2-NaCl system (**Table 2**; **Figures 12–14**).

The coexistence of Type A (aqueous-carbonic) and Type B (aqueous) fluid inclusions allows to estimate the depth of ore formation using the method of intersecting of the isochores based on the CO_2–H_2O–NaCl system. Using the CO_2 density formulae of the state of the isochores of Span and Wagner (1996) and the H_2O density isochores of Steele-MacInnis et al. (2012), and the pressure conditions of Sterner and Pitzer (1994), the bulk composition and density of fluid inclusions of these gold deposits were determined as below. The isochores of the Type A (aqueous-carbonic) and Type B (aqueous) fluid inclusions were plotted using the Roedder and Bodnar (1980) and Bowers and Helgeson (1983) state of equations, respectively (**Figure 15**).

The trapping pressures of fluid inclusions have been determined using CO_2-rich inclusions in quartz veins of the Kunzeik and Zibyaung deposits. The bulk densities vary from 0.53 to 0.91 g/cm^3 and the densities of CO_2 range between 0.53 and 0.77 g/cm^3 (**Table 2**; **Figure 15**). The Types A and B fluid inclusions from the Kunzeik deposit indicate that the deposit was formed at 376–246°C and 54–164 MPa (**Figure 15**), and for Zibyaung, it is estimated to be 358–242°C and 53–156 MPa (**Figure 15**). These data suggest a temperature and pressure variation during the ore-forming process. Depending on the pressure, the depth of mineralization was estimated. Given that studied areas are in a compressive orogenic environment, the formula can be used to estimate the metallogenic depth by lithostatic pressure: $H = P/(\rho \times g)$ (ρ represents average density of rocks, such as 2.70 g/cm^3). These pressures correspond to the

TABLE 3 | Comparative table showing characteristics of the Shwetagun, Kunzeik and Zibyaung deposits with other orogenic gold deposits in Myanmar and worldwide.

Name of Deposit/ Prospect	Location and Geologic Setting	Host Rocks	Mineralization Styles	Alterations	Metal Associations	Ore Fluid Systems, Temperature and Salinity	Regional Peak Metamorphism Events	Age of Host Terranes	References
Golden Mile	Kalgoorlie, Western Australia	Black shale, slate, basalts, and dolerite	Quartz vein and stockwork	Carbonation, Sericitization Sulfidation	Cu, Fe, As, Pb, Zn, Bi, Sb, Mo, Te, Ag, Au	H_2O-CO_2±CH_4-NaCl 200–400 °C (0.5–10 wt% eqiv. NaCl)	Lower greenschist Archean	Archean	Shackleton et al., 2003; Groves et al., 1998, 2003; Goldfarb et al., 2001, 2005
Western Lachlan Orogen	Victoria SE Australia	Slates, massive sandstone	Laminated or ribbon banded quartz vein disseminated–stockwork-breccia systems	Carbonation, Sericitization Sulfidation	Cu, Fe, As, Pb, Zn, Sb, Mo, Ag, Au	H_2O-CO_2±CH_4-NaCl 200–400°C (2–10 wt% eqiv. NaCl)	Zeolite– Lower amphibolite Devonian	Upper Cambrian–Lower Devonian	Groves et al., 1998, 2003; Goldfarb et al., 2001, 2005; Bierlein et al., 2004
Buller Terrane	Western South Island, New Zealand	Massive siltstone and sandstone	Ribbon texture banded vein shear-zone-related quartz lodes gold	Carbonation, Sericitization Sulfidation	Cu, Fe, As, Ag, Au	H_2O-CO_2±CH_4-NaCl 152–293°C (3.5–7.2 wt% eqiv. NaCl)	Lower greenschist Devonian	Upper Cambrian–Middle Ordovician	Bierlein et al., 2004; Groves et al., 1998,2003; Goldfarb et al., 2001, 2005
Meguma Terrane	Nova Scotia, Canada	Slate, argillite or meta-sandstones	Laminated bedding-parallel veins	Carbonate Sericite Chlorite Sulphidation	Cu, Fe, As, Pb, Sn, Ag, Au	H_2O-CO_2±CH_4-NaCl 300–400°C (<10 wt% eqiv. NaCl)	Lower greenschist–Upper amphibolite Devonian	Upper Cambrian–Upper Ordovician	Groves et al., 1998, 2003; Goldfarb et al., 2001, 2005; Bierlein et al., 2004
Main Divide and Pingfengshan	Slate Belt, Taiwan	Mudstones, Siltstones, sandstones and micaceous schists	Chloritic fissure, ankeritic, massive veins	Ankeritic, Chlorite–Calcite	Cu, Fe, As, Pb, Zn, Ag, Au	H_2O-NaCl 172–350°C 0.8–5.4 wt% eqiv.NaCl	Sub-greenschist to Lower greenschist post-Miocene	Eocene–Miocene	Craw et al. (2010)
Phayaung Taung	Mergui Belt, Southern Myanmar	Phyllite, schist, and quartzite	Sulfide quartz vein	Silicification Phyllic/Sericitic, Chloritization Oxidation	Cu, Fe, As, Pb, Zn, Bi, Te, Ag, Au	H_2O-NaCl 243–426°C (0.4–8.4 wt% eqiv. NaCl)	Lower greenschist –Upper Amphibolite Lower Jurassic - Eocene	Upper Carboniferous to Lower Permian	Win Phyo et al., 2016; Ye Myint Swe et al., 2017
Modi Taung	Mergui Belt, Southern Myanmar	Mudstone, graywacke, and slate	Laminated or ribbon banded quartz vein, Sheeted vein	Carbonation, Sericitization Sulfidation	Cu, Fe, As, Pb, Zn, Ag, Au	Unknown	Lower greenschist Lower Jurassic - Eocene	Upper Carboniferous to Lower Permian	Mitchell et al., 2004; Traynor et al., 2015, 2017
Shwetagun	Mergui Belt, Southern Myanmar	Mudstone, graywacke, and slate	Laminated or sheeted quartz vein	Sulfidation Sericitization Chloritization, Silicification	Cu, Fe, As, Pb, Zn, Ag, Au	H_2O-NaCl 250–335°C (0.2–4.6 wt% eqiv. NaCl)	Lower greenschist Lower Jurassic - Eocene	Upper Carboniferous to Lower Permian	This study
Shwegyin	Mergui Belt, Southern Myanmar	Slate, phyllite, schist, and quartzite	Sulfide quartz vein, Sheeted vein	Carbonation, Sericitization Sulfidation	Cu, Fe, As, Pb, Zn, Ag, Au	H_2O-CO_2±CH_4-NaCl 245–411 (1.5–7.0 wt% eqiv. NaCl)	Lower greenschist –Upper Amphibolite Lower Jurassic - Eocene	Upper Carboniferous to Lower Permian	May Thwe Aye et al. (2017)
Kunzeik	Mergui Belt, Southern Myanmar	Slate, biotite granite, granodiorite	Sulfide quartz vein, stockwork	Sulfidation Sericitization	Cu, Fe, Mo, Ag, Au	H_2O ~ CO_2 –NaCl	Lower greenschist Lower Jurassic - Eocene	Upper Carboniferous to Lower Permian	Myo Kyaw Hlaing et al., 2019bib_Kyaw_et_al_2019; This study

(Continued on following page)

TABLE 3 | (*Continued*) Comparative table showing characteristics of the Shwetagun, Kunzeik and Zibyaung deposits with other orogenic gold deposits in Myanmar and worldwide.

Name of Deposit/ Prospect	Location and Geologic Setting	Host Rocks	Mineralization Styles	Alterations	Metal Associations	Ore Fluid Systems, Temperature and Salinity	Regional Peak Metamorphism Events	Age of Host Terranes	References
						*a 273–356°C (1.6–4.6 wt% eqiv. NaCl) *b 246–376°C (1.1–10.7 wt% eqiv. NaCl)			
				Chloritization, Silicification					
Zibyaung	Mergui Belt, Southern Myanmar	Mudstone, Slate and schist	Sulfide quartz vein	Sulfidation	Cu, Fe, Pb, Zn, Ag, Au	H_2O-CO_2-NaCl	Lower greenschist –Upper Amphibolite	Upper Carboniferous to Lower Permian	Myo Kyaw Hlaing et al., 2019; This study
				Sericitization		*a 312–348°C (4.6–9.6 wt% eqiv. NaCl)			
				Chloritization, Silicification		*b 242–358°C (0.9–11.8 wt% eqiv. NaCl)	Lower Jurassic - Eocene		
Meyon	Mergui Belt, Southern Myanmar	Sandstone and carbonaceous mudstones, Slate	Stratabound, Sulfide quartz vein	Carbonation, Sericitization	Cu, Fe, As, Zn, Ag, Au	H_2O-CO_2±CH_4-NaCl 240–370°C (5–12 wt% eqiv. NaCl)	Lower greenschist –Upper Amphibolite	Upper Carboniferous to Lower Permian	Zaw Naing Oo et al. (2010); Zaw Naing Oo and Khin Zaw (2009), Zaw (2015), Zaw (2017)
				Sulfidation			Lower Jurassic - Eocene		
				Albitization					

*Notes: *a = Aqueous-carbonic fluid inclusions, *b = Aqueous fluid inclusions.*

calculated depths of ore formation between 2.0 and 6.1 km under lithostatic conditions. These temperatures, depth and recorded alteration mineralogy in the Kunzeik and Zibyaung deposits are consistent with mesozonal orogenic gold deposits elsewhere (e.g., Groves et al., 1998, 2003; McCuaig and Kerrich 1998; Goldfarb et al., 2001, 2005; Elmer et al., 2006).

Metallogenic Implications

The structural setting of the MB is ideal for generation of orogenic gold deposits as described by Groves et al. (2003), which includes a first-order structure that focuses and channelizes metal-bearing fluids and neighboring second-order and possibly third-order structures that contain fluids, and the major processes comprising the formation of quartz veins and metal deposition around them (e.g., Goldfarb et al., 2001; Groves and Bierlein, 2007). A large number of orogenic or lode gold deposits are structurally-controlled by brittle-ductile shear zones and faults and are distinguished by fault-valve nature (Sibson et al., 1988; Cox et al., 1991; Cox 1995; Robert et al., 1995; Dubé and Gosselin, 2007). In the case of the MB, these structures can be defined by the transcrustal, first-order, the second-order shear zone, and reactivated Papun fault system located in the middle to south of the belt and the third-order structures semi-parallel to the fault zone and hosting the gold mineralization (**Figures 2**, **16**).

The Shwetagun gold-bearing quartz veins and, in particular, the Zibyaung and Khunzeik veins in MB show a structural relationship between the first-order structures, mostly N-S to NNE-NNW oriented, and second order one trending NW–SE. The fault-valve model for orogenic gold deposits represents the cyclic fluctuation in fluid pressures, from lithostatic to hydrostatic, due to episodic shear stress (Sibson et al., 1988; Ridley 1993; Robert et al., 1995; Cox et al., 1995, 2001; Sibson and Scott 1998; Kisters et al., 2000; Oliver and Bons 2001; Groves et al., 2003). The available sulfur isotopic data along MB indicate that the $\delta^{34}S$ values of pyrite range from →2.80–4.43‰ in Meyon, (Zaw Naing Oo and Khin Zaw, 2009) and a range of +1.33–4.75‰ in Modi Taung (Traynor et al., 2015). These data suggest that the sulfur responsible for gold mineralization is likely to have been derived from a dominant magmatic source with a possible other minor fluid such as metamorphic fluid (e.g., Wyman et al., 2016; Groves et al., 2020).

The age of the gold district of Modi Taung-Nankwe was stratigraphically considered between the Upper Permian and the Middle Jurassic (Mitchell et al., 2004). They considered that it was an orogenic style gold, linking its genesis to the crustal fluids generated during the metamorphism of the MMB (Mitchell et al., 2004; Gardiner et al., 2016). This metamorphism was defined as Jurassic in age, contemplating this age for gold mineralization (Mitchell et al., 2004). However, Searle et al. (2007) suggested a much younger age of Paleogene for peak metamorphism in MMB. Here, at Modi Taung, the Theingi vein is cut by a 20 m wide dyke, and the Shwesin and Momi Taung veins are cut by small dykes and sills (Mitchell et al., 2004; Traynor et al., 2015, 2017). LA ICP-MS U-Pb zircon dating of granitoid unit intruding the host sequence of the Modi Taung gold deposit yielded 95 ± 30 Ma and the age of the

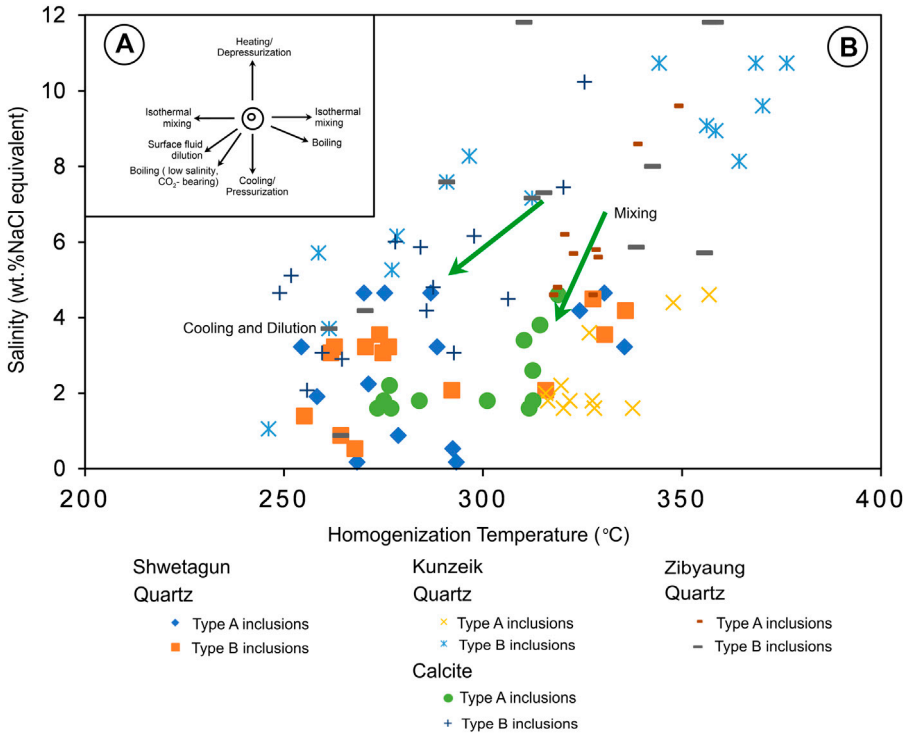

FIGURE 14 | Diagram showing **(A)** typical trends in the T_h (°C)–Salinity space caused by various fluid evolution mechanisms (from Wilkinson, 2001), and **(B)** variations of homogenization temperature and salinity of fluid inclusions with hydrothermal fluid evolution from Shwetagun, Kunzeik, and Zibyaung. The green arrows indicate that both temperature and salinity are decreasing.

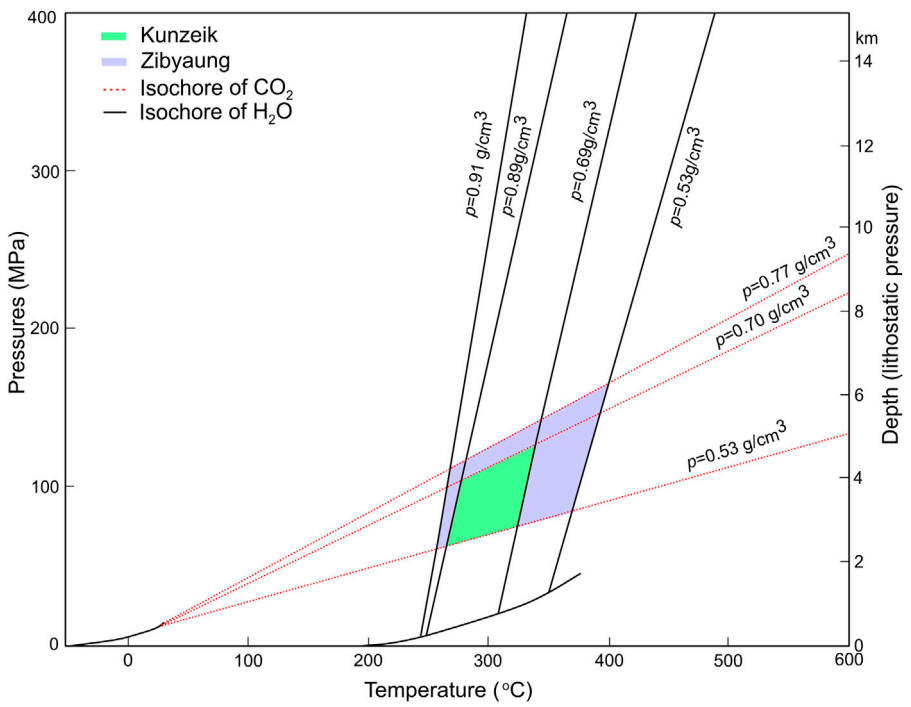

FIGURE 15 | P-T diagram displaying isochores of the minimum and maximum densities of two types of fluid inclusions (modified from Roedder and Bodnar, 1980; Bowers and Helgeson, 1983). Figure indicates the density values (in g/cm^3) for respective inclusions. P-T estimation by intersecting isochores of Type A (aqueous-carbonic) (dashed lines) and Type B (aqueous) (solid lines) inclusions.

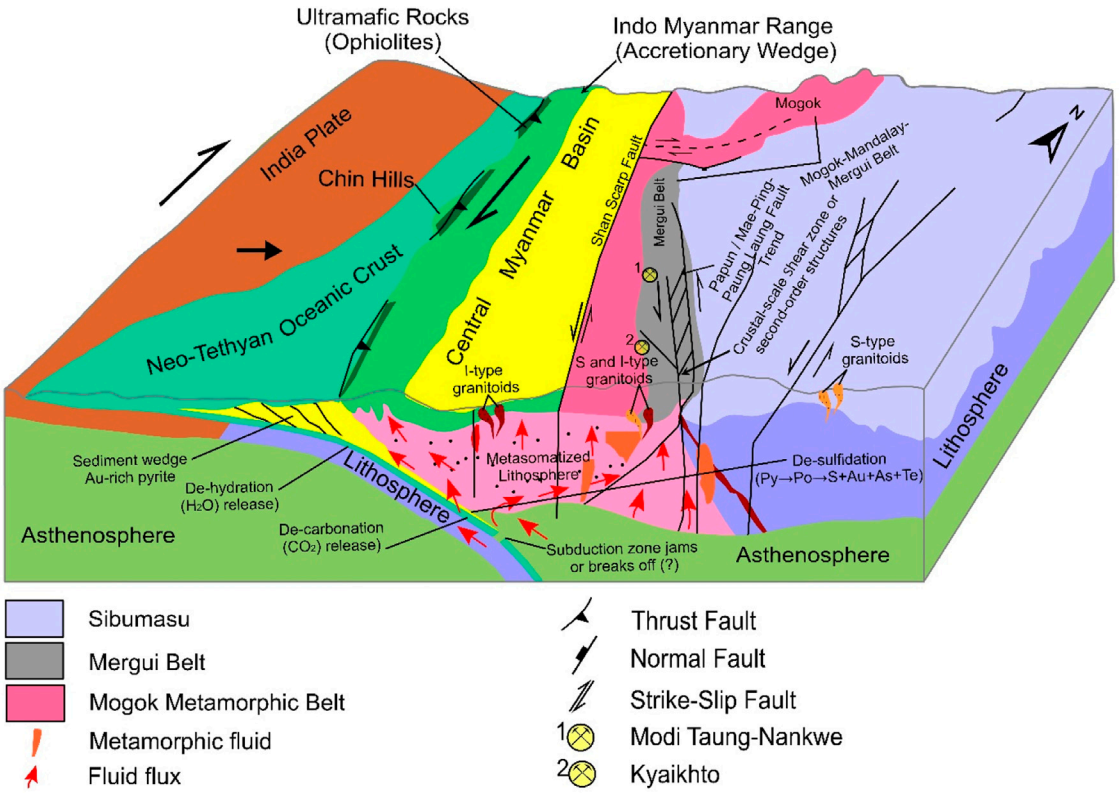

FIGURE 16 | Tectonic setting of Myanmar during Lower Cretaceous to Oligocene depicting formation and evolution of gold mineralization in the framework of subduction and collision-based model for ore-fluid source(s) of the orogenic gold deposits of Mergui Belt (Modified after Gardiner et al., 2016, 2018; Groves et al., 2019, 2020).

andesitic dyke cross-cutting the mineralization by LA ICP-MS U-Pb dating of apatite was determined to be 49 ± 1 Ma (Traynor et al., 2015, 2017). Further work on U-Pb dating of zircon from the cross-cutting dyke is required to ascertain the robust age for the dyke intrusion, the age of the orogenic gold mineralization at the Shwetagun deposit in the Modi Taung-Nankwe gold district appeared that it was formed relatively late. The age of mineralization of the Meyon is proposed to be Lower Cretaceous to Paleogene and may have been consistent with deformation and metamorphism as being structurally-controlled and linked to movement along the Papun Fault Zone (**Figure 16**; Zaw Naing Oo and Khin Zaw, 2009, 2017).

During the Lower Cretaceous to Oligocene, Myanmar was influenced by at least two main orogenic events (Cretaceous and Eocene), which may have contributed to widespread regional metamorphism which is possibly linked to gold mineralization in the MB (e.g., Mitchell et al., 2004; Gardiner et al.,2014; Khin Zaw et al., 2014a; Zaw Naing Oo and Khin Zaw, 2015; Khin Zaw, 2017; Gardiner et al., 2018). Gold veins were formed during the ascent of metamorphic fluids following the uplifting and prograde metamorphism of the entire MMMB. The generation of this high-grade metamorphic process was associated with the subduction and collision of the India-Eurasia Plate (Khin Zaw et al., 2014b). Thus, we suggest that the age of mineralization for the orogenic gold deposits in the MB may have been Lower Cretaceous to Oligocene, and the emplacement of the mineralizing fluids was associated with retrograde metamorphism of the MMMB and dehydration at a depth of 2–12 km (e.g., Mitchell et al., 2004).

All the evidence presented for the orogenic gold deposits of the MB also suggest that the mineralizing fluids were derived from multi-sources and the initial ore-forming fluids were thought to be either due to fluids produced by metamorphic devolatization and/or mixed with magmatic fluid (e.g., Wyman et al., 2016; Groves et al., 2020). These multi-sourced fluids may have been transported from the deep crust to the shallower level via first-order faults during the evolution of the ore fluid, especially in the late stages of ore precipitation (e.g., Kerrich and Fyfe, 1981; Higgins and Kerrich, 1982; Cameron and Hattori, 1987; Phillips and Powell, 1993; Mikucki, 1998; Diamond, 2001; Wilkinson, 2001). The derivation of the ore fluids from the supracrustal rocks below the continental crust is widely accepted for the source (s) of orogenic gold deposits (Phillips and Powell, 2010; Goldfarb and Santosh, 2014), either from the subducted slab, with overlying oceanic sediments, or from the lithosphere below (**Figure 16**; Groves and Santosh, 2015). Dehydration and metamorphism within the oceanic crust and sediments have been well-observed mechanisms for producing abundant aqueous-carbonic and low-salinity fluids, as

documented in orogenic gold deposits from fluid inclusions that induce massive energy and mass transport, culminating in the fractionation of mobile and even immobile elements (Pearce and Peate, 1995; Ridley and Diamond, 2000; Spandler et al., 2003).

In this context, the MB is a tectonic component of the Sibumasu terrane during the Jurassic to Cretaceous when the main tectonic transition from N-S compression to NNE-SSW shearing was progressively occurred. The large-scale circulation of fluids, granitic magmatism and metallogenesis took place during the Lower Cretaceous to Oligocene in the MB, as a result of which the initial ore fluids of the orogenic gold deposits were likely formed by dehydration, decarbonization and desulfidation of the subducting Neo-Tethys slab (**Figure 16**; e.g., Ridley and Diamond 2000; Phillips and Powell, 2010; Goldfarb and Santosh, 2014; Yardley and Bodnar, 2014; Khin Zaw et al., 2014b; Yardley and Cleverley 2015; Groves and Santosh, 2016; Groves et al., 2020).

CONCLUSION

This integrated study provided a framework for the genesis and metallogenic significance of gold mineralization in the Mergui Belt as below:

1. The comparison of the two gold systems in Mergui Belt suggests that the gold deposits are mainly hosted by the mudstone, slaty mudstone, greywacke sandstone, slate, and slaty phyllite of Mergui Group (dominantly of Carboniferous age), and are structurally-controlled by the NNE-NNW trending faults system. Hydrothermal alteration processes of various extents developed along the NNE-NNW trending structures and the alteration process was dominated by chloritization, sericitization, carbonatization, silicification. The most common sulfides are pyrite, sphalerite, chalcopyrite, and galena with native gold and electrum.
2. Comparing the fluid inclusion characteristics, evolution of fluid and depth estimation indicate that the ore fluids are composed of high temperature, low salinity, low CO_2, aqueous–carbonic fluid belonging to a H_2O-CO_2-NaCl system. The ore-bearing fluids are considered to have derived from dominantly of metamorphic with possible magmatic fluid inputs. Intersection of isochores of fluid inclusions in this study suggests that gold deposits were formed under the PT-depth conditions comparable to the global orogenic gold systems as evidenced by temperatures ranging from (242–376°C) to pressure (53–164 MPa) corresponding to a depth at around 2.0 and 6.1 km under lithostatic conditions.
3. The regional tectonic setting provided by comparison of the Shwetagun, Zibyaung and Khunzeik deposits raises the question of the timing of gold mineralization in Mergui Belt. The orogenic gold deposits in the Mergui Belt may have been genetically linked to the deformation and metamorphism of the host Paleozoic sequence at the time of the inferred Cretaceous to Oligocene age of mineralization. This prolonged tectonic and metallogenic event was associated with the subduction of the Neo-Tethys oceanic slab (**Figure 16**).
4. Additional ongoing controversies remain to investigate the origin of the gold deposits of the Mergui Belt in Myanmar whether the source of the gold was derived from deeper mantle or recycling and remobilization of crustal gold syngenetically accumulated in back arc basins of Sinbumasu. Further systematic investigations are required to successfully establish the relative timing of magmatism, metamorphism, and to address the importance of ore-forming processes involved in orogenic gold mineralization and future exploration.

DATA AVAILABILITY STATEMENT

The original contributions presented in the study are included in the article/Supplementary Material, further inquiries can be directed to the corresponding author.

AUTHOR CONTRIBUTIONS

This work is a late result of the first author's Master thesis (Department of Geology, University of Yangon, 2013) combined with some part from Ph. D thesis (Department of Earth Resources Engineering, Kyushu University, 2019). All authors finally endorsed the findings and contributed to the final manuscript.

FUNDING

This study has been financially supported by the Japan International Cooperation Agency (JICA) SHIGEN NO KIZUNA program for the PhD scholarship and the Frontiers Fee Support Grant No. DSC-11032129724PRD).

ACKNOWLEDGMENTS

Special thanks are due to the editor and two reviewers for their insightful suggestions and reviews, which significantly improved the manuscript.

REFERENCES

Aung Zaw Myint., Khin Zaw., Ye Myint Swe., Yonezu, K., Cai, Y., Manaka, T., et al. (2017). "Geochemistry and Geochronology of Granites Hosting the Mawchi Sn-W deposit, Myanmar: Implications for Tectonic Setting and Granite Emplacement," in *Myanmar: Geology, Resources and Tectonics*. Editors A. J.Barber, Khin Zaw, and M. J. Crow (London: The Geological Society, Memoir), 48, 387–402. doi:10.1144/m48.17

Barley, M. E., Doyle, M. G., Khin, Z., Pickard, A. L., and Rak, P. (2003). Jurassic–Miocene Magmatism and Metamorphism in the Mogok Metamorphic Belt and the India-Eurasia Collision in Myanmar. *Tectonics* 22, 1–11. doi:10.1029/2002tc001398

Barley, M. E., and Groves, D. I. (1992). Supercontinent Cycles and the Distribution of Metal Deposits through Time. *Geol* 20, 291–294. doi:10.1130/0091-7613(1992)020<0291:scatdo>2.3.co;2

Bender, F. (1983). *Geology of Burma*. Stuttgart: Gebrüder Borntraeger, 295.

Bierlein, F. P., and Crowe, D. E. (2000). Phanerozoic Orogenic Lode Gold Deposits. *Rev. Econ. Geol.* 13, 103–140. doi:10.5382/Rev.13.03

Bierlein, F. P., Christie, A. B., and Smith, P. K. (2004). A Comparison of Orogenic Gold Mineralisation in central Victoria (AUS), Western South Island (NZ) and Nova Scotia (CAN): Implications for Variations in the Endowment of Palaeozoic Metamorphic Terrains. *Ore Geology. Rev.* 25, 125–168. doi:10.1016/j.oregeorev.2003.09.002

Bierlein, F. P., Groves, D. I., and Cawood, P. A. (2009). Metallogeny of Accretionary Orogens - the Connection between Lithospheric Processes and Metal Endowment. *Ore Geology. Rev.* 36, 282–292. doi:10.1016/j.oregeorev.2009.04.002

Bierlein, F. P., Groves, D. I., Goldfarb, R. J., and Dubé, B. (2006). Lithospheric Controls on the Formation of Provinces Hosting Giant Orogenic Gold Deposits. *Miner Deposita* 40, 874–886. doi:10.1007/s00126-005-0046-2

Bodnar, R. J. (1993). Revised Equation and Table for Determining the Freezing point Depression of H2O-Nacl Solutions. *Geochimica et Cosmochimica Acta* 57, 683–684. doi:10.1016/0016-7037(93)90378-a

Bowers, T. S., and Helgeson, H. C. (1983). Calculation of the Thermodynamic and Geochemical Consequences of Nonideal Mixing in the System H2O-CO2-NaCl on Phase Relations in Geologic Systems: Equation of State for H2O-CO2-NaCl Fluids at High Pressures and Temperatures. *Geochimica et Cosmochimica Acta* 47, 1247–1275. doi:10.1016/0016-7037(83)90066-2

Cameron, E. M., and Hattori, K. (1987). Archean Gold Mineralization and Oxidized Hydrothermal Fluids. *Econ. Geol.* 82, 1177–1191. doi:10.2113/gsecongeo.82.5.1177

Campbell McCuaig, T., and Kerrich, R. (1998). P-T-t-deformation-fluid Characteristics of Lode Gold Deposits: Evidence from Alteration Systematics. *Ore Geology. Rev.* 12, 381–453. doi:10.1016/s0169-1368(98)80002-4

Chhibber, H. L. (1934). *The mineral Resources of Burma*. London: Macmillan.

Cobbing, E. J., Pitfield, P., Darbyshire, D., and Mallick, D. (1992). *The Granites of the Southeast Asian Tin Belt*, 10. London: Overseas Memoirs of the British Geological Survey.

Cobbing, E. J., Mallick, D. I. J., Pitfield, P. E. J., and Teoh, L. H. (1986). The Granites of the Southeast Asian Tin belt. *J. Geol. Soc.* 143, 537–550. doi:10.1144/gsjgs.143.3.0537

Collins, P. L. F. (1979). Gas Hydrates in CO 2 -bearing Fluid Inclusions and the Use of Freezing Data for Estimation of Salinity. *Econ. Geol.* 74, 1435–1444. doi:10.2113/gsecongeo.74.6.1435

Connolly, J. A. D. (2010). The Mechanics of Metamorphic Fluid Expulsion. *Elements* 6 (3), 165–172. doi:10.2113/gselements.6.3.165

Cox, S. F., Knackstedt, M. A., and Braun, J. (2001). "Principles of Structural Control on Permeability and Fluid Flow in Hydrothermal Systems," in *Structural Controls on Ore Genesis*. Editors J. P. Richards and R. M. Tosdal (Littleton, CO: Rev. Econ. Geol.), 14, 1–24. doi:10.5382/Rev.14.01

Cox, S. F., Etheridge, M. A., Cas, R. A. F., and Clifford, B. A. (1991). Deformational Style of the Castlemaine Area, Bendigo-Ballarat Zone: Implications for Evolution of Crustal Structure in central Victoria. *Aust. J. Earth Sci.* 38, 151–170. doi:10.1080/08120099108727963

Cox, S. F. (1995). Faulting Processes at High Fluid Pressures: an Example of Fault Valve Behavior from the Wattle Gully Fault, Victoria, Australia. *J. Geophys. Res.* 100 (B7), 12841–12859. doi:10.1029/95jb00915

Cox, S. F., Sun, S. S., Etheridge, M. A., Wall, V. J., and Potter, T. F. (1995). Structural and Geochemical Controls on the Development of Turbidite-Hosted Gold Quartz Vein Deposits, Wattle Gully Mine, central Victoria, Australia. *Econ. Geol.* 90, 1722–1746. doi:10.2113/gsecongeo.90.6.1722

Craw, D., Upton, P., Yu, B.-S., Horton, T., and Chen, Y.-G. (2010). Young Orogenic Gold Mineralisation in Active Collisional Mountains, Taiwan. *Miner Deposita* 45, 631–646. doi:10.1007/s00126-010-0297-4

Davies, R. S., Groves, D. I., and Standing, J. G. (2019). Litho-structural Controls on Orogenic Gold Deposits within the Sandstone Greenstone belt, Yilgarn Craton, Western Australia: Implications for Exploration Targeting. *Appl. Earth Sci.* 1–10. doi:10.1080/25726838.2019.1674540

Diamond, L. W. (2001). Review of the Systematics of CO2-H2O Fluid Inclusions. *Lithos* 55, 69–99. doi:10.1016/S0024-4937(00)00039-6

Dubé, B., and Gosselin, P. (2007). "Greenstone-hosted Quartz-Carbonate Vein Deposits," in *Mineral Deposits of Canada: A Synthesis of Major Deposit-Types, District Metallogeny, the Evolution of Geological Provinces, and Exploration Methods: Geological Association of Canada, Mineral Deposits*. Editor W. D. Good fellow (India: Division, Spec. Publ.), 5, 49–73.

Elmer, F. L., White, R. W., and Powell, R. (2006). Devolatilization of Metabasic Rocks during Greenschist-Amphibolite Facies Metamorphism. *J. Metamorph. Geol.* 24, 497–513. doi:10.1111/j.1525-1314.2006.00650.x

Gardiner, N. J., Robb, L. J., and Searle, M. P. (2014). The Metallogenic Provinces of Myanmar. *Appl. Earth Sci. (Trans. Inst. Min. Metall. B)* 123, 1. doi:10.1179/1743275814y.0000000049

Gardiner, N. J., Robb, L. J., Morley, C. K., Searle, M. P., Cawood, P. A., Whitehouse, M. J., et al. (2016). The Tectonic and Metallogenic Framework of Myanmar: A Tethyan mineral System. *Ore Geology. Rev.* 79, 26–45. doi:10.1016/j.oregeorev.2016.04.024

Gardiner, N. J., Searle, M. P., Morley, C. K., Robb, L. J., Whitehouse, M. J., Roberts, N. M. W., et al. (2018). The Crustal Architecture of Myanmar Imaged through Zircon U-Pb, Lu-Hf and O Isotopes: Tectonic and Metallogenic Implications. *Gondwana Res.* 62, 27–60. doi:10.1016/j.gr.2018.02.008

Gardiner, N. J., Searle, M. P., Robb, L. J., and Morley, C. K. (2015). Neo-Tethyan Magmatism and Metallogeny in Myanmar - an Andean Analogue? *J. Asian Earth Sci.* 106, 197–215. doi:10.1016/j.jseaes.2015.03.015

Goldfarb, R. J., Ayuso, R., Miller, M. L., Ebert, S. W., Marsh, E. E., Petsel, S. A., et al. (2004). The Late Cretaceous Donlin Creek Gold Deposit, Southwestern Alaska: Controls on Epizonal Ore Formation. *Econ. Geology.* 99, 643–671. doi:10.2113/gsecongeo.99.4.643

Goldfarb, R. J., Baker, T., Dube, B., Groves, D. I., Hart, C. J. R., and Gosselin, P. (2005). "Distribution, Character, and Genesis of Gold Deposits in Metamorphic Terranes," in *Economic Geology 100th Anniversary Volume*. Editors J. W. Hedenquist, J. F. H. Thompson, R. J. Goldfarb, and J. P. Richards (Littleton: Society of Economic Geologists Inc.), 407–450.

Goldfarb, R. J., Groves, D. I., and Gardoll, S. (2001). Orogenic Gold and Geologic Time: a Global Synthesis. *Ore Geol. Rev.* 18 (1-2), 1–75. doi:10.1016/s0169-1368(01)00016-6

Goldfarb, R. J., and Groves, D. I. (2015). Orogenic Gold: Common or Evolving Fluid and Metal Sources through Time. *Lithos* 233, 2–26. doi:10.1016/j.lithos.2015.07.011

Goldfarb, R. J., and Santosh, M. (2014). The Dilemma of the Jiaodong Gold Deposits: Are They Unique? *Geosci. Front.* 5, 139–153. doi:10.1016/j.gsf.2013.11.001

Groves, D. I., and Bierlein, F. P. (2007). Geodynamic Settings of mineral deposit Systems. *J. Geol. Soc.* 164, 19–30. doi:10.1144/0016-76492006-065

Groves, D. I., Goldfarb, R. J., Gebre-Mariam, M., Hagemann, S. G., and Robert, F. (1998). Orogenic Gold Deposits: a Proposed Classification in the Context of Their Crustal Distribution and Relationship to Other Gold deposit Types. *Ore Geology. Rev.* 13, 7–27. doi:10.1016/s0169-1368(97)00012-7

Groves, D. I., Goldfarb, R. J., Robert, F., and Hart, C. J. R., Jr. (2003). Gold Deposits in Metamorphic Belts: Overview of Current Understanding,Outstanding Problems, Future Research, and Exploration Significance. *Econ. Geology.* 98, 1–29. doi:10.2113/gsecongeo.98.1.1

Groves, D. I., Santosh, M., Deng, J., Wang, Q., Yang, L., and Zhang, L. (2019). A Holistic Model for the Origin of Orogenic Gold Deposits and its Implications for Exploration. *Miner Deposita* 55, 275–292. doi:10.1007/s00126-019-00877-5

Groves, D. I., Santosh, M., Goldfarb, R. J., and Zhang, L. (2018). Structural Geometry of Orogenic Gold Deposits: Implications for Exploration of World-Class and Giant Deposits. *Geosci. Front.* 9, 1163–1177. doi:10.1016/j.gsf.2018.01.006

Groves, D. I., and Santosh, M. (2015). Province-scale Commonalities of Some World-Class Gold Deposits: Implications for mineral Exploration. *Geosci. Front.* 6, 389–399. doi:10.1016/j.gsf.2014.12.007

Groves, D. I., and Santosh, M. (2016). The Giant Jiaodong Gold Province: the Key to a Unified Model for Orogenic Gold Deposits? *Geosci. Front.* 7, 409–417. doi:10.1016/j.gsf.2015.08.002

Groves, D. I., Santosh, M., and Zhang, L. (2020). A Scale-Integrated Exploration Model for Orogenic Gold Deposits Based on a mineral System Approach. *Geosci. Front.* 11, 719–738. doi:10.1016/j.gsf.2019.12.007

Groves, D. I. (1993). The Crustal Continuum Model for Late-Archaean Lode-Gold Deposits of the Yilgarn Block, Western Australia. *Mineral. Deposita* 28, 366–374. doi:10.1007/bf02431596

Hagemann, S., and Cassidy, K. (2000). Archean Orogenic Lode Gold Deposits. *Rev. Econ. Geol.* 13, 9–68. doi:10.5382/Rev.13.01

Higgins, N. C., and Kerrich, R. (1982). Progressive 18O Depletion during CO2 Separation from a Carbon Dioxide-Rich Hydrothermal Fluid: Evidence from the Grey River Tungsten deposit, Newfoundland. *Can. J. Earth Sci.* 19, 2247–2257. doi:10.1139/e82-198

Kerrich, R., and Fyfe, W. S. (1981). The Gold-Carbonate Association: Source of CO2, and CO2 Fixation Reactions in Archaean Lode Deposits. *Chem. Geology.* 33, 265–294. doi:10.1016/0009-2541(81)90104-2

Kerrich, R., Goldfarb, R., Groves, D., and Garwin, S. (2000). The Geodynamics of World-Class Gold Deposits: Characteristics, Space–Time Distribution, and Origins. *Rev. Econ. Geol.* 13, 501–551. doi:10.5382/Rev.13.15

Khin Zaw (1990). Geological, Petrogical and Geochemical Characteristics of Granitoid Rocks in Burma: with Special Reference to the Associated WSn Mineralization and Their Tectonic Setting. *J. Southeast Asian Earth Sci.* 4, 293–335. doi:10.1016/0743-9547(90)90004-w

Khin Zaw (2017). "Chapter 24 Overview of Mineralization Styles and Tectonic-Metallogenic Setting in Myanmar," in *Myanmar: Geology, Resources and Tectonics*. Editors A. J. Barber, K. Zaw, and M. J. Crow (London: Geological Society. Memoirs), 48, 531–556. doi:10.1144/M48.24

Khin Zaw (2019). "Tectonic and Metallogenic Significance of Orogenic Gold Deposits in mainland SE Asia" in The Society Of Resource Geology Annual Meeting, Tokyo, Japan, June 26–28, 2019.

Khin Zaw., Meffre, S., Lai, C.-K., Burrett, C., Santosh, M., Graham, I., et al. (2014a). Tectonics and Metallogeny of mainland Southeast Asia - A Review and Contribution. *Gondwana Res.* 26, 5–30. doi:10.1016/j.gr.2013.10.010

Khin Zaw., Santosh, M., and Graham, I. T. (2014b). Tectonics and Metallogeny of mainland SE Asia: Preface. *Gondwana Res.* 26, 1–4. doi:10.1016/j.gr.2014.01.005

Khin Zaw., Makoundi, C., and Hai Thanh Tran. (2018). "Metallogenic Significance of Sediment-Hosted/orogenic Gold Deposits in mainland SE Asia: Keynote Address," in *Geosea XV: Regional Congress on Geology, Mineral and Energy Resources of SE Asia* (Ha Noi, Vietnam), 16–17.

Kisters, A. F. M., Kolb, J., Meyer, F. M., and Hoernes, S. (2000). Hydrologic Segmentation of High-Temperature Shear Zones: Structural, Geochemical and Isotopic Evidence from Auriferous Mylonites of the Renco Mine, Zimbabwe. *J. Struct. Geology.* 22, 811–829. doi:10.1016/s0191-8141(00)00006-7

Large, R. R., Bull, S. W., and Maslennikov, V. V. (2011). A Carbonaceous Sedimentary Source-Rock Model for Carlin-type and Orogenic Gold Deposits. *Econ. Geology.* 106, 331–358. doi:10.2113/econgeo.106.3.331

Large, R. R., Maslennikov, V. V., Robert, F., Danyushevsky, L. V., and Chang, Z. (2007). Multistage Sedimentary and Metamorphic Origin of Pyrite and Gold in the Giant Sukhoi Log deposit, Lena Gold Province, Russia. *Econ. Geology.* 102, 1233–1267. doi:10.2113/gsecongeo.102.7.1233

Mackenzie, M. J. (1999). *Report on the Exploration Progress in Block 3/13 for the Period January 1998 to December 1998*. Myanmar Burma: Palmer Resources Ltd. Myanmar (Burma) Project, 1–67.

May Thwe Aye., Myo Kyaw Hlaing.,Yonezu, K., and Watanabe, K. (2017). Fluid Inclusion Study of Shwegyin Gold deposit, Proceedings of the 7th Asia Africa Mineral Resources Conference, November 20-24, 2017, Bago Region, Myanmar. 157–160.

McCuaig, T. C., Beresford, S., and Hronsky, J. (2010). Translating the mineral Systems Approach into an Effective Exploration Targeting System. *Ore Geology. Rev.* 38, 128–138. doi:10.1016/j.oregeorev.2010.05.008

Mikucki, E. J. (1998). Hydrothermal Transport and Depositional Processes in Archean Lode Goldsystems: a Review. *Ore Geol. Rev.* 13, 307–321. doi:10.1016/S0169-1368(97)00025-5

Mitchell, A., Chung, S.-L., Oo, T., Lin, T.-H., and Hung, C.-H. (2012). Zircon U-Pb Ages in Myanmar: Magmatic-Metamorphic Events and the Closure of a Neo-Tethys Ocean? *J. Asian Earth Sci.* 56, 1–23. doi:10.1016/j.jseaes.2012.04.019

Mitchell, A. H. G. (2018). *Geological Belts, Plate Boundaries, and mineral Deposits in Myanmar*. Oxford: Elsevier, 509. doi:10.1016/B978-0-12-803382-1.01001-4

Mitchell, A. H. G., Nyunt, Htay., Asua, C., Deiparine, L., Aung, Khine., and Po., Sein. (1999). *Geological Settings of Gold Districts in Myanmar*. Berlin: Pacrim Berli Seminar.

Mitchell, A. H. G., Ausa, C. A., Deiparine, L., Hlaing, T., Htay, N., and Khine, A. (2004). The Modi Taung-Nankwe Gold District, Slate Belt, central Myanmar: Mesothermal Veins in a Mesozoic Orogen. *J. Asian Earth Sci.* 23, 321–341. doi:10.1016/S1367-9120(03)00138-X

Mitchell, A. H. G., Htay, M. T., Htun, K. M., Win, M. N., Oo, T., and Hlaing, T. (2007). Myint Thein Htay., Kyaw Min Htun., Myint Naing Win., Thura Oo., and Tin HlaingRock Relationships in the Mogok Metamorphic belt, Tatkon to Mandalay, central Myanmar. *J. Asian Earth Sci.* 29, 891–910. doi:10.1016/j.jseaes.2006.05.009

Mitchell, A. H. G. (1977). Tectonic Settings for Emplacement of Southeast Asian Tin Granites. *Bgsm* 9, 123–140. doi:10.7186/bgsm09197710

Myo Kyaw Hlaing (2013). *Geology and Geochemical Characteristics of Gold Mineralization at Shwetagun Area, Yemethin Township, Mandalay Region*. Myanmar: University of Yangon. M.Sc Thesis.

Myo Kyaw Hlaing., Aung Zaw Myint., Tindell, T., and May Thwe Aye (2019). Gold Mineralization in the Kyaikhto District, Mon State, Southern Myanmar. *Open J. Geol.* 9, 29–42. doi:10.4236/ojg.2019.91003

Oliver, N. H. S., and Bons, P. D. (2001). Mechanisms of Fluid Flow and Fluid-Rock Interaction in Fossil Metamorphic Hydrothermal Systems Inferred from Vein wall Rock Patterns, Geometry and Microstructure. *Geofluids.* 1, 137–162. doi:10.1046/j.1468-8123.2001.00013.x

Pearce, J. A., and Peate, D. W. (1995). Tectonic Implications of the Composition of Volcanic Arc Magmas. *Annu. Rev. Earth Planet. Sci.* 23, 251–285. doi:10.1146/annurev.ea.23.050195.001343

Phillips, G. N. (1993). Metamorphic Fluids and Gold. *Mineral. Mag.* 57 (388), 365–374. doi:10.1180/minmag.1993.057.388.02

Phillips, G. N., and Evans, K. A. (2004). Role of CO2 in the Formation of Gold Deposits. *Nature* 429, 860–863. doi:10.1038/nature02644

Phillips, G. N., and Powell, R. (2010). Formation of Gold Deposits: a Metamorphic Devolatilization Model. *J. Metamorph. Petrol.* 28, 689–718. doi:10.1111/j.1525-1314.2010.00887.x

Phillips, G. N., and Powell, R. (2009). Formation of Gold Deposits: Review and Evaluation of the Continuum Model. *Earth-Science Rev.* 94, 1–21. doi:10.1016/j.earscirev.2009.02.002

Phillips, G. N., and Powell, R. (1993). Link between Gold Provinces. *Econ. Geol.* 88, 1084–1098. doi:10.2113/gsecongeo.88.5.1084

Poulsen, K. H., Robert, F., and Dubé, B. (2000). Geological Classification of Canadian Gold Deposits. *Geol. Surv. Can. Bull.* 540, 106. doi:10.4095/211094

Ridd, M. F., and Watkinson, I. (2013). The Phuket-Slate Belt Terrane: Tectonic Evolution and Strike-Slip Emplacement of a Major Terrane on the Sundaland Margin of Thailand and Myanmar. *Proc. Geologists' Assoc.* 124, 994–1010. doi:10.1016/j.pgeola.2013.01.007

Ridley, J. R., and Diamond, L. W. (2000). "Fluid Chemistry of Lode-Gold Deposits and Implications for Genetic Models," in *Reviews in Economic Geology: Gold in 2000*. Editors S. G. Hagemann and P. Brown (Littleton, Colorado, United States: Society of Economic Geologists), 13, 141–162.

Ridley, J. (1993). The Relations between Mean Rock Stress and Fluid Flow in the Crust: with Reference to Vein- and Lode-Style Gold Deposits. *Ore Geology. Rev.* 8, 23–37. doi:10.1016/0169-1368(93)90026-u

Robert, F., Boullier, A.-M., and Firdaous, K. (1995). Gold–quartz Veins in Metamorphic Terranes and Their Bearing on the Role of Fluids in Faulting. *J. Geophys. Res. Solid Earth* 100 (87), 861–879. doi:10.1029/95jb00190

Robert, F., and Poulsen, K. H. (2001). "Vein Formation and Deformation in Greenstone Gold Deposits," in *Structural Control on Ore Genesis*. Editors J. P. Richards and R. M. Tosdal (Edmonton, AB: Rev. Econ. Geol.), 14, 111–155. doi:10.5382/Rev.14.05

Robert, F., Poulson, H. K., Cassidy, K. F., and Hodgson, J. C. (2005). "Gold Metallogeny of the superior and Yilgarn Cratons," in *Economic Geology 100th Anniversary* (Littleton, Colorado, United States: Society of Economic Geologists), 1001–1033. doi:10.5382/av100.30

Roedder, E., and Bodnar, R. J. (1980). Geologic Pressure Determinations from Fluid Inclusion Studies. *Annu. Rev. Earth Planet. Sci.* 8, 263–301. doi:10.1146/annurev.ea.08.050180.001403

Roedder, E. (1984). Fluid Inclusions. *Rev. Mineralogy* 12, 644pp. doi:10.1515/9781501508271

Schwartz, M. O., Rajah, S. S., Askury, A. K., Putthapiban, P., and Djaswadi, S. (1995). The Southeast Asian Tin belt. *Earth-Science Rev.* 38, 95–293. doi:10.1016/0012-8252(95)00004-t

Searle, M. P., Noble, S. R., Cottle, J. M., Waters, D. J., Mitchell, A. H. G., Tin, Hlaing., et al. (2007). Tectonic Evolution of the Mogok Metamorphic belt, Burma (Myanmar) Constrained by U-Th-Pb Dating of Metamorphic and Magmatic Rocks. *Tectonics* 26. doi:10.1029/2006tc002083

Shackleton, J. M., Spry, P. G., and Bateman, R. (2003). Telluride Mineralogy of the Golden Mile Deposit, Kalgoorlie, Western Australia. *Can. Mineral.* 41, 1503–1524. doi:10.2113/gscanmin.41.6.1503

Sibson, R. H., Robert, F., and Poulsen, K. H. (1988). High-angle Reverse Faults, Fluid-Pressure Cycling, and Mesothermal Gold-Quartz Deposits. *Geol* 16, 551–555. doi:10.1130/0091-7613(1988)016<0551:harffp>2.3.co;2

Sibson, R. H., and Scott, J. (1998). Stress/fault Controls on the Containment and Release of Overpressured Fluids: Examples from Gold-Quartz Vein Systems in Juneau, Alaska; Victoria, Australia and Otago, New Zealand. *Ore Geology. Rev.* 13, 293–306. doi:10.1016/s0169-1368(97)00023-1

Span, R., and Wagner, W. (1996). A New Equation of State for Carbon Dioxide Covering the Fluid Region from the Triple-Point Temperature to 1100 K at Pressures up to 800 MPa. *J. Phys. Chem. Reference Data* 25, 1509–1596. doi:10.1063/1.555991

Spandler, C., Hermann, J. r., Arculus, R., and Mavrogenes, J. (2003). Redistribution of Trace Elements during Prograde Metamorphism from Lawsonite Blueschist to Eclogite Facies; Implications for Deep Subduction-Zone Processes. *Contrib. Mineralogy Petrology* 146 (2), 205–222. doi:10.1007/s00410-003-0495-5

Steele-MacInnis, M., Lecumberri-Sanchez, P., and Bodnar, R. J. (2012). HokieFlincs_H2O-NaCl : A Microsoft Excel Spreadsheet for Interpreting Microthermometric Data from Fluid Inclusions Based on the PVTX Properties of H 2 O-NaCl. *Comput. Geosciences* 49, 334–337. doi:10.1016/j.cageo.2012.01.022

Sterner, S. M., and Pitzer, K. S. (1994). An Equation of State for Carbon Dioxide Valid from Zero to Extreme Pressures. *Contr. Mineral. Petrol.* 117, 362–374. doi:10.1007/bf00307271

Tomkins, A. G. (2013). On the Source of Orogenic Gold. *Geol* 41, 1255–1256. doi:10.1130/focus122013.1

Tomkins, A. G. (2010). Windows of Metamorphic Sulfur Liberation in the Crust: Implications for Gold deposit Genesis. *Geochimica et Cosmochimica Acta* 74 (11), 3246–3259. doi:10.1016/j.gca.2010.03.003

Traynor, J., Eskine, T., Khin ZawLarge, R. R., Makoundi, C., and Knight, J. (2015). Geology and Mineralization Characteristics of the Modi Taung Orogenic Gold deposit, Central Myanmar. Proceedings of the SEG Conference, 27–30 September 2015, Hobart, Australia, CD-ROM.

Traynor, J., Eskine, T., Zaw, K., Large, R. R., Makoundi, C., and Tin Tun (2017). *Geology and Mineralisation Characteristics of the Modi Taung Orogenic Gold deposit, Central Myanmar:* Inaugural Conference On Applied Earth Sciences In Myanmar and Neighboring Regions. Yangon, Myanmar: Myanmar Applied Earth Sciences Association, 118.

Wilkinson, J. J. (2001). Fluid Inclusions in Hydrothermal Ore Deposits. *Lithos* 55, 229–272. doi:10.1016/S0024-4937(00)00047-5

Win Phyo., Yonezu, K., and Watanabe, K. (2016). Ore-forming Conditions of Metasedimentary Rock-Hosted Gold Mineralization, Phayaung Taung Area, Mandalay Region, central Myanmar. *Proc. Int. Symp. Earth Sci. Technology*, 314–319.

Wyman, D. A., Cassidy, K. F., and Hollings, P. (2016). Orogenic Gold and the mineral Systems Approach: Resolving Fact, Fiction and Fantasy. *Ore Geology. Rev.* 78, 322–335. doi:10.1016/j.oregeorev.2016.04.006

Yardley, B. W. D., and Bodnar, R. J. (2014). Fluids in the continental Crust. *Geochemical Perspect.* 3 (1), 123pp. doi:10.7185/geochempersp.3.1

Yardley, B. W. D., and Cleverley, J. S. (2015). "The Role of Metamorphic Fluids in the Formation of Ore Deposits," in *Ore Deposits in an Evolving Earth*. Editors G. R. T. Jenkin, P. A. J. Lusty, I. McDonald, M. P. Smith, A. J. Boyce, and J. J. Wilkinson (London: Geological Soci. Spec. Publ), 393, 117–134. doi:10.1144/sp393.5*Geol. Soc. Lond. Spec. Publications*

Ye Myint Swe., Cho Cho Aye., and Khin Zaw. (2017). "Chapter 25 Gold Deposits of Myanmar," in *Myanmar: Geology, Resources, and Tectonics*. Editors A. J. Barber, K. Zaw, and M. J. Crow (London: The Geological Society, Memoirs, London), 48, 557–572. doi:10.1144/M48.25

Zaw Naing Oo., and Khin Zaw. (2009). Geology and Mineralization Characteristics of Meyon Gold deposit, Mon State, Southern Myanmar. Proceedings of the 11th Regional Congress on Geology, Mineral and Energy resources of Southeast Asia (GEOSEA), 8–10 June, Kuala Lumpur, Malaysia, 32.

Zaw Naing Oo., Khin Zaw., and Mernagh, T. (2010). Geological Setting and Nature of Mineralization at Meyon Gold deposit, Mon State, Myanmar. Proceedings of the 13th quadrennial international association on genesis of ore deposits (IAGOD) symposium, 6–9 April, 2010. CD-ROM, Adelaide.

Zaw Naing Oo., and Khin Zaw. (2015). Geological Setting and Nature of Mineralization at Meyon Gold deposit, Southern Myanmar. Proceedings of the SEG Conference, 27–30 September 2015, Hobart, Australia, CD-ROM.

Zaw Naing Oo., and Khin Zaw. (2017). *Geological Setting and Nature of Mineralization at Meyon Gold Deposit, Southern Myanmar:* Inaugural Conference On Applied Earth Sciences In Myanmar and Neighboring Regions. Yangon, Myanmar: Myanmar Applied Earth Sciences Association, 111.

Conflict of Interest: The authors declare that the research was conducted in the absence of any commercial or financial relationships that could be construed as a potential conflict of interest.

Publisher's Note: All claims expressed in this article are solely those of the authors and do not necessarily represent those of their affiliated organizations or those of the publisher, the editors, and the reviewers. Any product that may be evaluated in this article, or claim that may be made by its manufacturer, is not guaranteed or endorsed by the publisher.